N O T I C E

NASA

Technical Memorandum 82162

Monitoring Tropical Cyclone Intensity Using Wind Fields Derived from Short-Interval Satellite Images

Edward B. Rodgers and R. Cecil Gentry

JULY 1981

National Aeronautics and
Space Administration

Goddard Space Flight Center
Greenbelt, Maryland 20771

MONITORING TROPICAL CYCLONE INTENSITY

USING WIND FIELDS

DERIVED FROM SHORT-INTERVAL SATELLITE IMAGES

Edward B. Rodgers[1]

R. Cecil Gentry[2]

[1] Laboratory for Atmospheric Sciences (GLAS), Goddard Space Flight Center,
National Aeronautics and Space Administration, Greenbelt, MD 20771.

[2] Department of Physics and Astronomy, Clemson University, Clemson, SC 29631.

CONTENTS

TABLES

MONITORING TROPICAL CYCLONE INTENSITY
USING WIND FIELDS
DERIVED FROM SHORT-INTERVAL SATELLITE IMAGES

Edward B. Rodgers[1]

R. Cecil Gentry[2]

ABSTRACT

Rapid scan visible images from the Visible Infrared Spin Scan Radiometer (VISSR) sensor on board SMS-2 and GOES-1 have been used to derive high resolution upper and lower tropospheric environmental wind fields around three western Atlantic tropical cyclones (Caroline, August 1975, Anita, August and September 1977, and Ella, September 1978). These wind fields were used to derive upper and lower tropospheric areal mean relative vorticity and their differences, the net relative angular momentum balance and upper tropospheric mass outflow. These kinematic parameters have been shown by studies using composite rawinsonde data to be strongly related to tropical cyclone formation and intensity changes. Also, the role of forced synoptic scale subsidence in tropical cyclone formation was examined.

The three case studies showed that satellite-derived lower and upper tropospheric wind fields can be used to monitor and possibly predict tropical cyclone formation and intensity changes. These kinematic analyses showed that future changes in tropical cyclone intensity are mainly related to the "spin-up" of the storms by the net horizontal transport of relative angular momentum caused by convergence of cyclonic vorticity in the lower troposphere and to a lesser extent the divergence of anticyclone vorticity in the upper troposphere. For the three cases studied, the upper tropospheric environmental circulation helped to influence changes of storm intensity by hindering

---

[1] Laboratory for Atmospheric Sciences (GLAS), Goddard Space Flight Center, National Aeronautics and Space Administration, Greenbelt, MD 20771.

[2] Department of Physics and Astronomy, Clemson University, Clemson, SC 29631.

or enhancing the storm's outflow. It is also apparent from the Anita case study that satellite-derived wind fields can assist in the detection of the occurrence of tropical cyclone formation in regions where concentrated upper tropospheric convergence overlies a lower tropospheric cyclonic vortex.

MONITORING TROPICAL CYCLONE INTENSITY USING WIND FIELDS

DERIVED FROM SHORT-INTERVAL SATELLITE IMAGES

Edward B. Rodgers[1]

R. Cecil Gentry[2]

1. INTRODUCTION

It is well known that the damage caused by a tropical cyclone varies with at least the square of the wind speed. (Howard et al., 1972). Therefore, tropical cyclone intensity and intensity changes are important subjects that have attracted many investigators. Some have listed a qualitative group of necessary but non-sufficient conditions for tropical cyclone formation and intensification (Riehl, 1954). Numerical models that can predict intensity changes have not been developed sufficiently enough to use real data effectively. Modelers who have tried to make quantitative use of real data have encountered problems in obtaining sufficiently accurate data.

The data problem is serious because most intensity changes take place over the open ocean far removed from dense observing networks. Data collected by hurricane reconnaissance aircraft have been very useful. There have been numerous case studies of tropical cyclones by a number of researchers (Riehl and Malkus, 1961; LaSeur and Hawkins, 1963; Hawkins and Rubsam, 1968; and Hawkins and Imbembo, 1976) using aircraft reconnaissance data that have related storm intensity to inner core thermodynamic parameters (i.e., D-values, temperature anomalies) and kinematic parameters (i.e., maximum winds). However, the flight data have rarely been sufficient to provide a good three-dimensional description of both the tropical cyclone and its environment. In addition, there is a tendency due to economical constraints in recent years to further reduce reconnaissance aircraft flights into tropical cyclones, particularly those that are at large distance from landfall.

[1]Laboratory for Atmospheric Sciences (GLAS), Goddard Space Flight Center, National Aeronautics and Space Administration, Greenbelt, MD 20771.

[2]Department of Physics and Astronomy, Clemson University, Clemson, SC 29631.

Rawinsonde data provide a better vertical representation of the tropical cyclone structure, dynamics, and energetics, especially for the outer environmental regions of the storm. However, it has usually been necessary to composite rawinsonde data from many storms in order to have sufficient coverage. McBride, 1979; Nunez and Gray, 1977; Frank, 1977a and b; Arnold, 1977; Zehr, 1976; and Erickson, 1977 have composited 20 years of rawinsonde data from the western Pacific and 14 years from the West Indies within and outside of tropical cyclones. The data were composited according to storm intensity over an area of $15°$ latitude radius from the storm center in $1°$ latitude steps and in 19 vertical levels at 50 mb increments. Although this technique cannot be used to monitor the thermodynamic and dynamic parameters of individual tropical cyclones, it is an extremely useful method to assess what mean parameters are the most important to monitor in order to better understand the process of tropical cyclone formation and intensification.

However, because of sampling difficulties associated with reconnaissance aircraft flights and the rawinsonde measurements, there is an obvious need to emphasize satellite remote sensing techniques for monitoring tropical cyclone formation and intensity changes.

There have been several techniques that have utilized satellite remote sensing. Dvorak (1975) has used cloud pattern analyses qualitatively for monitoring and predicting tropical cyclone intensity. This method, however, has its maximum difficulty with abnormal storms. A more quantitative study by Gentry, et al. (1980) has related tropical cyclone cloud-top temperatures (an index of latent heat release (LHR)) to storm intensity. These cloud-top temperatures were obtained from infrared window measurements made by sensors on board the Nimbus satellites. LHR has also been inferred from the passive microwave measurements at 19.35 GHz from the Electrically Scanning Microwave Radiometer on board Nimbus-5 (ESMR-5) and related to storm intensity and intensity changes (Adler and Rodgers, 1977; Rodgers and Adler, 1981). Nimbus-6 Scanning Microwave Spectrometer (SCAMS) measured upper tropospheric temperature anomalies near the center of tropical cyclones have been related to storm intensity by hydrostatically estimating minimum surface pressure and surface winds outside the radius of maximum winds (Kidder, 1978, 1980). These satellite-based techniques, however, have not demonstrated sufficient accuracy and reliability

2

to replace aircraft reconnaissance. This is because the tropical cyclone intensity parameters are indirectly measured. The assumptions that are necessary for the calculation of tropical cyclone parameters (particularly LHR) are not well understood and the spatial and temporal resolutions of the observations are inadequate.

At the earlier stages of tropical cyclone development, the previously mentioned satellite-derived measurements (i.e., SCAMS, ESMR-5) are monitoring the tropical cyclone temperature and latent heat properties which have been shown by Gray (1975, 1979) to be unrelated to tropical cyclone formation and intensification. At the mature stage, however, these satellite-derived thermal parameters are more indicative of storm intensification.

At all stages of development, the dynamics of the storm and surrounding atmosphere seems highly correlated with storm intensification. From rawinsonde data McBride (1979); McBride and Gray (1978); and Frank (1977a) have shown that there is a strong relationship between the net radial mass flux within the surrounding environment and tropical cyclone formation and intensity variation. Also Zehr, 1976; Erickson, 1977; and McBride, 1979 showed that the relative vorticity difference between the upper and lower troposphere within the surrounding environment is related to storm formation and intensification. This radiosonde-derived correlation is encouraging, since direct measurements of the wind fields within the inner core of tropical cyclones is usually not feasible using satellite remote sensing techniques because of the storm's dense cloud cover and heavy rainfall. However, satellite remote sensing techniques can be used to derive wind fields surrounding the storm's central dense overcast (CDO). Satellite measurement of the environmental wind fields have been done routinely by using a cloud tracking procedure that utilizes successive geosynchronous satellite infrared and visible images obtained at approximately 20 to 30 minute intervals. Although these techniques are limited in vertical resolution and to areas where there are cloud tracers, satellites are uniquely capable of supplying synoptic wind data within the environment surrounding the storm near the cloud base and cirrus levels where there is the greatest concentration of radial mass flux in and out of the storm. Synoptic observations of the environmental wind flow are needed to observe the asymmetries of storm's outflow. Black and Anthes (1971) have shown from satellite-derived

3

upper tropospheric wind fields that these asymmetries are strongly related to the large scale fluxes of energy and momentum, and therefore, to the storm's intensity change.

Fujita and Tecson, 1974; Smith, 1975; Erickson, 1974; and Hawkins, 1976 have also used satellite-derived wind fields to estimate tropical cyclone intensity. However, since the wind fields were derived from successive geosynchronous images at approximately 30 minute intervals, the best success in the studies was found in relating satellite upper tropospheric kinematics within the storm's environment to storm intensity. Less success was found in the lower troposphere. This was because the life expectancy of the cloud tracers was usually too short to be observed with any continuity using 30-minute interval images. However, it has been shown by Rodgers et al. (1979) that by observing limited areas of the globe every 3 to 7.5 minutes using the SMS/GOES Visible Infrared Spin Scan Radiometer (VISSR), the continuity of observing the cloud tracers is greatly improved. A factor of 10 (5) increase in the number of useful cloud tracers were obtained using the 3 to 7.5 minute interval VISSR data as compared to using images at intervals of 30 (15) minutes. Therefore, within the immediate tropical cyclone environment during the day, the VISSR visible channel (spatial resolution approximately 1 km) provided useful mesoscale lower tropospheric wind fields surrounding the tropical cyclone. At the cirrus level, the higher temporal resolution VISSR images also made it easier to find cloud tracers even within the storm's CDO because of the greater resolution.

It is the purpose of this paper to utilize SMS-2 and GOES-1 rapid scan visible images (3 to 7.5 minute intervals) to obtain cloud motion winds in order to investigate the dynamical relationship between the large-scale upper and lower tropospheric circulation surrounding tropical cyclones and the inner core characteristics. It is also planned to determine the feasibility of monitoring and possibly predicting tropical cyclone intensity changes using the satellite-derived winds. These analyses will be compared with the composite rawinsonde results cited earlier that have shown relationships between winds in the upper and lower troposphere and current and future cyclone intensity.

4

Three tropical cyclones were examined where rapid-scan images were available at 1300, 1600, and 1900 GMT on three consecutive days for each storm. The storms were Caroline (August 28, 29, and 30, 1975), Anita (August 30 and 31 and September 1, 1977), and Ella (September 1, 2, and 3, 1978). They were the only storms for which there were multiple days of rapid-scan observations. Only one of the time intervals on each day will be discussed since little variation was found between the kinematic analysis during each time period during the day.

2. ANALYSIS

Hasler, et al. (1979) have shown from aircraft observations within the oceanic trade wind region that the translation of convective clouds approximates the ambient flow at the cloud base level and that cirrus cloud translation approximates the mean ambient flow in the cirrus layer. Movement of cumulus 3-15 km in diameter with a base at 960 mb and tops at 650 mb had vector differences of 1.3 ms^{-1} at the cloud base, while cirrus had vector difference from the ambient flow at the cloud layer of 1.6 ms^{-1}. It is not known from direct observations whether the translation of convective clouds immediately outside a tropical cyclone CDO represents the ambient flow at the cloud base level. However, considering the small vertical shear up to the upper tropospheric level within a tropical cyclone environment (Frank, 1977a), the convective cloud tracers are likely to be representative of the ambient flow at the cloud base level.

At the cirrus level, there is large vertical shear so that the height determination of cirrus using an infrared technique is usually not accurate. Moreover, the emissivity of the cloud is usually less than one and has large variability. For these case studies all cirrus clouds were assigned to 200 mb, which was assumed to be the level of maximum outflow. A more accurate determination of cirrus heights for future cases can be made using stereographic techniques (Hasler, 1981).

The clouds were tracked on NASA's interactive Atmospheric and Oceanographic Information Processing System (AOIPS). Discussion of the technique used to obtain satellite-derived winds and a brief description of AOIPS can be found in Rodgers, et al. (1979).

The Lackman method, which is part of the AOIPS software, was used to objectively smooth the satellite winds to grid points. The Lackman method is similar to the Cressman technique (Cressman, 1959), except that it also weights wind data by shadowing and eliminates the ballooning effect in data-poor areas by using previously calculated grid points as further data input. The grid spacing for the objective analysis was 0.4° latitude, while the length of the influence radius was taken to be 2.01 times the grid spacing.

Wind data obtained from the available aircraft reconnaissance flights at an altitude of about 0.5 km at the approximate time of the satellite observations (within ±2h) were used to augment the lower tropospheric satellite-derived winds. Aircraft-derived winds were particularly helpful in the case of tropical cyclone Anita. For example, in the southeastern quadrant of the storm at approximately 333 km radius from the center, dense cirrus made it impossible to track cumulus clouds in the lower troposphere. In this quadrant the aircraft-derived winds were used to produce a more realistic objectively analyzed wind field. By using the aircraft winds to augment the satellite-derived winds, the mean radial component of the wind changed sign in this quadrant (radial outward to radial inward) and the areal mean horizontal convergenced increased from $0.04 \times 10^{-5} s^{-1}$ to $2 \times 10^{-5} s^{-1}$. This value is more compatible with results from the composite rawinsonde observations at the same radius for storms of similar intensity. In areas where there were neither aircraft reconnaissance flights nor cloud tracers, wind data were introduced into the objective program after a subjective analysis was performed. Rawinsonde data were not used in the analysis since the measurements mainly occurred outside the area being analyzed.

To assess the validity of these rapid scan satellite-derived tropical cyclone wind fields, Hasler and Rodgers (1977) did a random error analysis on the high-resolution lower and upper tropospheric wind fields of three tropical cyclones (one of these storms was analyzed in this study). The error analysis consisted of: (1) the estimation of random errors in the cloud motion measurements by remeasuring cloud motion by a different analyst, and (2) artificially including a random number generator to perturb the x and y coordinates of the start and end points of each vector with an error that is normally distributed and has a variable standard deviation. The magnitude of the

vector difference was taken between the original vectors and the remeasured or perturbed vector.

Results from the error analysis showed that the largest two-thirds value of the magnitude of the difference for the repeatable error was 3.3 ms^{-1}. The difference was 3.1 ms^{-1} for the perturbation with a standard deviation of 1.0 pixel. This is twice the error that would be expected based on the spatial resolution of the satellite images and the total cloud-tracking time used to derive the wind fields. Objective analysis (Lackman/Cressman) of the wind fields gave a factor of 2 improvement in the wind errors at the grid points. The largest two-thirds value of the magnitude of the difference and relative vorticity fields using a standard deviation of 1.0 pixel vas no more than 5 percent of the maximum value of the original fields. The perturbed fields maintained their strongest divergence and vorticity features even when the perturbation was increased to a standard deviation of 2.4.

Other possible errors in obtaining satellite-derived wind fields using rapid-scan images are errors caused by: (1) navigation, (2) spatial and temporal resolution, and (3) cloud height computation. These errors have been discussed by Peslen (1980). By tracking lower tropospheric clouds over land using SMS-2 (0.9 km spatial and 5 minute temporal resolution visible images) and comparing the satellite-derived winds with rawinsonde data, Peslen (1980) found that the errors enumerated above were 1.7 ms^{-1}, 1.8 ms^{-1}, and 1.7 ms^{-1}, respectively. The total random and systematic error, including error between cloud motion and ambient flow, were estimated to be 4.6 ms^{-1} when based on the square root of the sum of the individual error sources. However, these errors should be larger than those found from cloud tracers over water because of the greater surface influence, shorter cloud lifetime, smaller cloud size, and the greater uncertainties of the cloud level. Also, as was demonstrated by Hasler and Rodgers (1977) the objectively analyzed wind errors and their first derivative for the cloud tracers over land should be smaller.

Comparisons of lower tropospheric cloud motions for tropical cyclones Eloise (22 September 1975), Caroline (30 August 1975), and Anita (31 August 1977), with winds measured 2-6h later at 0.5 to 1 km elevation from reconnaissance aircraft in approximately the same area showed an average speed difference of 2.5 ms^{-1} outside the CDO (Rodgers, et al., 1979). However, comparisons of this

7

type are less valid owing to the large time and space differences between the two measurements.

Fig. 1a shows an example of an upper tropospheric wind field derived from GOES-1 for hurricane Anita (1600 GMT, 1 September 1977) superimposed on the visible image of Anita. Figs. 1b, 1c, and 1d, respectively, show the objectively analyzed wind field using the Lackman technique and the radial and tangential components of the wind. The wind vectors represent the location and direction of motion of the tracked cloud. The length of the vector is proportional to wind speed. The solid (dashed) lines represent the inward (outward) radial wind component and the cyclonic (anticyclonic) tangential wind component. The circle of 222 km radius from the center of circulation encompasses the inner core area of the storm. The kinematic parameters are only valid outside the circle within the environmental circulation. The arrow at the center of the circle represents the approximate center of the storm circulation.

3. KINEMATIC PARAMETERS

The kinematic parameters that were computed within the environment surrounding the tropical cyclone and examined for expected useful relationships with tropical cyclone intensity changes are the relative vorticity difference between 900 and 200 mb (Zehr, 1976; Erickson, 1979; and McBride, 1979), the relative angular momentum balance (McBride, 1979; and Frank, 1977a), and upper tropospheric mass outflow (Holliday, 1977; Sadler, 1976; and Zehr, 1977). The relationships between the concentration of upper tropospheric subsidence and tropical cyclone formation (Arnold, 1979; Gray, 1975; Erickson, 1977; and Lopez, 1973) was also examined. These parameters were chosen for their reported strong relationship to tropical cyclone formation and intensity changes. Furthermore, these parameters can be realistically measured using satellite-derived wind fields.

a. The Difference Between Relative Vorticity at 900 and 200 mb

From composite studies of non-developing versus developing cloud clusters, McBride (1979) showed that the single most important environmental parameter for indicating tropical cyclone formation was the difference between relative vorticity in the lower and upper troposphere when
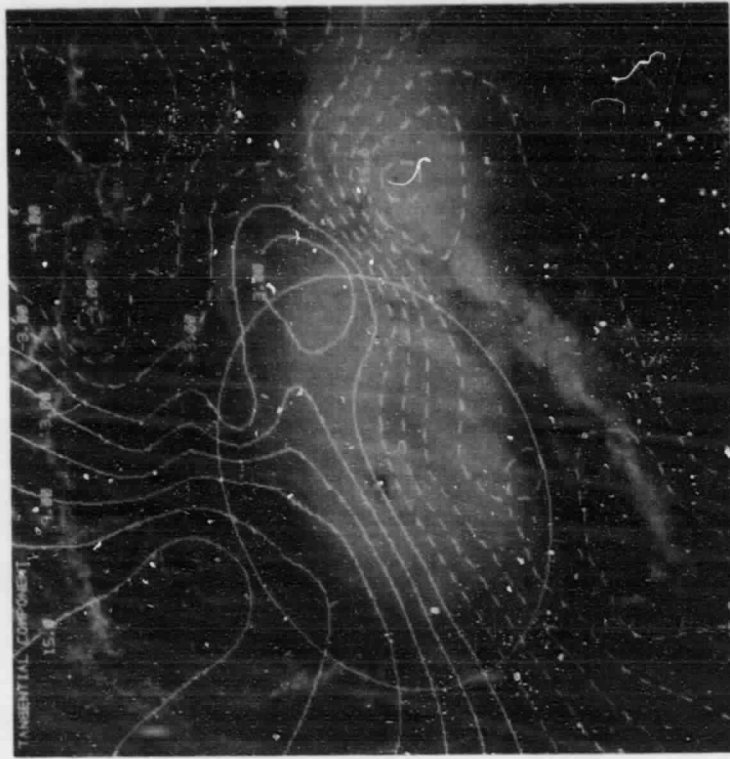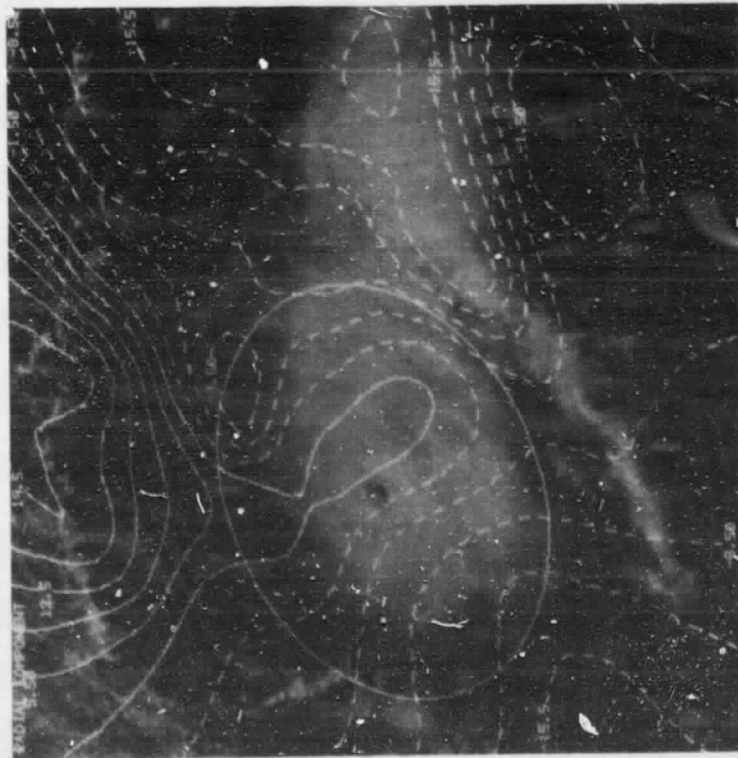
8
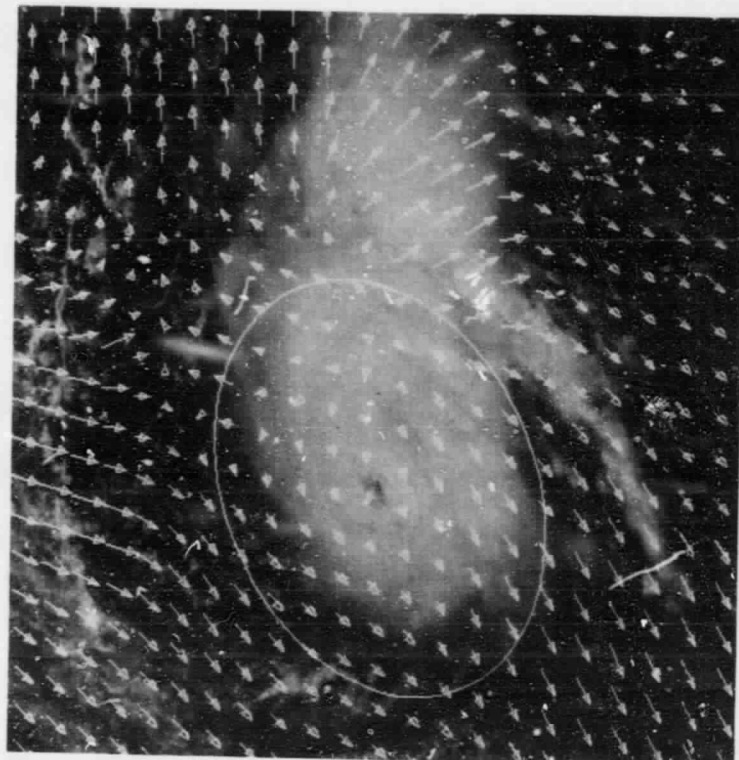
(b)
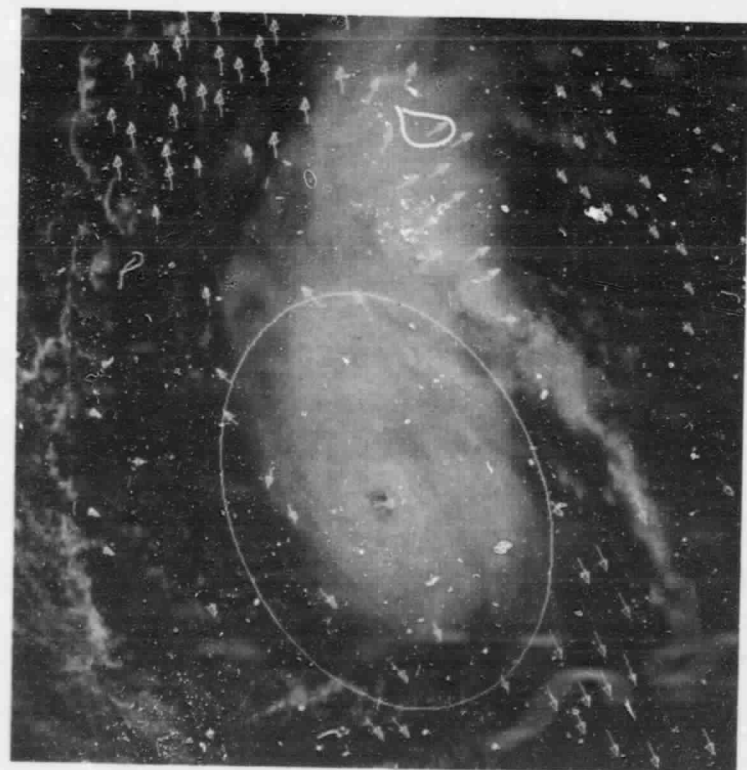
(a)

Figure 1. (a) Cirrus level wind field (wind speed in knots) derived from GOES-1 for hurricane Anita at 1600 GMT, 1 September 1977, (b) the objectively smoothed analyzed wind field (.4 km spacing) using the Lackman technique. (Continued)

(d)

(c)

Figure 1. (c) the radial, and (d) tangential wind component of the derived winds. See text for further explanation.

averaged over cylindrical areas with radii of 222 km and 444 km. He found that this difference was greater for developing systems. This result indicates that systems develop in regions having large-scale anticyclonic vorticity in the upper troposphere above an area of cyclonic vorticity in the lower troposphere. As a system intensifies, this difference increases. Thus, one should be able to determine tropical cyclone intensity changes by monitoring the environmental cyclonic relative vorticity in the lower troposphere, the anticyclonic relative vorticity in the upper troposphere, and the difference between these two parameters. Table 1 shows the McBride (1979) results. The table indicates the magnitude of the mean relative vorticity at 900 mb for a circle of 222 km radius from the center of the tropical cyclone and the relative vorticity difference between 900 and 200 mb at radii of 222 km and 444 km for systems that do and do not develop and for tropical cyclones at different intensities. These data were obtained from the composite of 14 years of north Atlantic rawinsonde data (McBride, 1979). The table indicates that areal mean relative vorticity either measured near the cloud base or obtained from the difference in areal mean relative vorticity between cloud base and cirrus level is related to tropical cyclone formation and intensity changes. Thus, tropical cyclone formation and intensity changes could be monitored from satellites if there is a sufficient coverage of cloud tracers.

TABLE 1

Areal Mean Relative Vorticity ($10^{-5}\,s^{-1}$)

Intensity	900 mb ζ_r 222 km	$(\zeta_{900} - \zeta_{200})$ 222 km	$(\zeta_{900} - \zeta_{200})$ 444 km
Non-developing Depression	2.4	2.0	5.5
Pre-hurricane Cloud Cluster	2.4	2.4	4.7
Pre-hurricane Depression	3.9	2.8	5.2
Intensifying Cyclone	4.8	4.2	9.8
Hurricane	7.3	5.2	10.8

To derive these parameters for the three storms using the satellite-derived winds, areal mean relative vorticity was computed at the cloud base and cirrus levels for a circular area with a radius of

11

333 km from the circulation center. The areal mean relative vorticity is defined as:

$$\zeta_r = \frac{1}{\Pi R^2} \int V_t \, ds \tag{1}$$

where R is the radius of the circle at which the relative vorticity is measured, V_t is the tangential component of the wind (positive cyclonic) and S is the surface along the boundary of the cylinder (Jordan, 1952).

b.   The Balance of Relative Angular Momentum

The storm's relative angular momentum balance provides an understanding of the effects exerted by the surrounding region of relative vorticity on the "spin-up" of the storm's volume and, therefore, storm intensification. To derive the balance of relative angular momentum for the three storms, computation was made for a cylinder of radius 333 km and height from the surface to 100 mb, using the total horizontal flux. The computation was similar to the technique developed by Frank (1977a).

$$\frac{\partial m}{\partial t} = \frac{1}{g} \int_{P_1}^{P_2} \int_{r_1}^{r_2} \int_0^{2\Pi} \left[(\overline{V_r V_t}) + (\overline{f R V_r}) \right] d\theta \, dr \, dP - \int_{r_1}^{r_2} \int_0^{2\Pi} \tau_{t,c} R^2 \, d\theta \, dr \tag{2}$$

Where:

R = Radius of cylinder

V_t = Tangential Velocity (positive cyclonic)

V_r = Radial Velocity (positive inwards)

m = Relative angular momentum ($V_t R$)

P = Pressure height of cylinder (surface to 100 mb)

r_1 = Inner radius of cylinder (center)

r_2 = Outer radius of cylinder (333 km)

$\tau_{t,0}$ = Surface stress term ($\rho C_D |V| V_t$)

$V = (v_t^2 + V_r^2)^{1/2} (ms^{-1})$

12

$$g \ = \ \text{Gravity } (9.8 \text{ ms}^{-2})$$

$$f \ = \ 14.56 \times 10^{-5} \ (\sin \phi \, s^{-1})$$

$$\phi \ = \ \text{Latitude}$$

$$\rho \ = \ \text{Density of Air } (1.2 \text{ kg m}^{-3} \times 10^{-3})$$

$$\overline{V_r Q} \ \approx \ \overline{V_r} \cdot \overline{Q} + \overline{V_r' \cdot Q'} \ = \ \text{Total horizontal flux of a mean quantity (Q) is equal to the flux}$$

of the quantity by the mean circulation and the horizontal eddy

flux. The bar denotes spatial averaging.

The equation states that the vertically integrated local change in angular momentum for a given

cylinder is equal to the net horizontal flux of relative angular momentum, the coriolis torque, and

the surface frictional dissipation.

To compute the angular momentum balance for a given cylinder, various assumptions are made.

First, storm motion is subtracted from the V_r and V_t wind components. Second, there is no vertical

flux of angular momentum above 100 mb. Third, 80 percent of the wind at the cloud base level is

used in the computation of the surface frictional dissipation term (Frank, 1977a). The last assumption

is that there is zero net mass divergence in the cylinder.

In order to assure zero mass divergence in a cylinder, it was first assumed for these case studies

that the V_r profile for a cylinder of radius 333 km corresponds to the V_r profile derived from the

composite rawinsonde data at 444 km radius from the center of western Atlantic hurricanes

(McBride, 1979). The composite rawinsonde V_r profile seen in Fig. 2a shows that the majority

of the outflow is concentrated between 300 and 100 mb with a maximum at 200 mb, the maximum

inflow is approximately constant from the surface to 800 mb and that there is little radial flow

between 800 and 300 mb. Secondly, based upon the composite rawinsonde V_r profile, it was

assumed that the V_r profile could be simulated from satellite-derived winds. It was assumed that

the satellite-derived V_r at the cirrus level represented the 200 mb V_r (providing that the maximum

outflow occurs at the cirrus level) and the satellite-derived V_r at the cloud base level represented

the constant V_r in the lower troposphere. In the middle troposphere, V_r was assumed to be zero.

Fig. 2b shows this simplified V_r profile. Finally, using the satellite-derived V_r profile, zero net
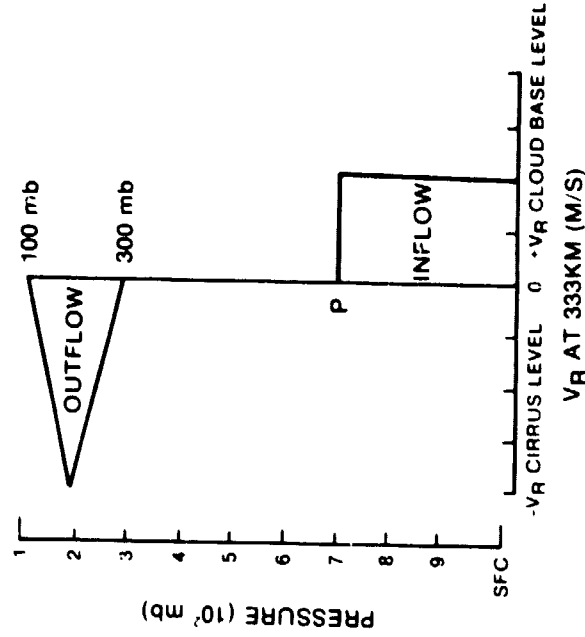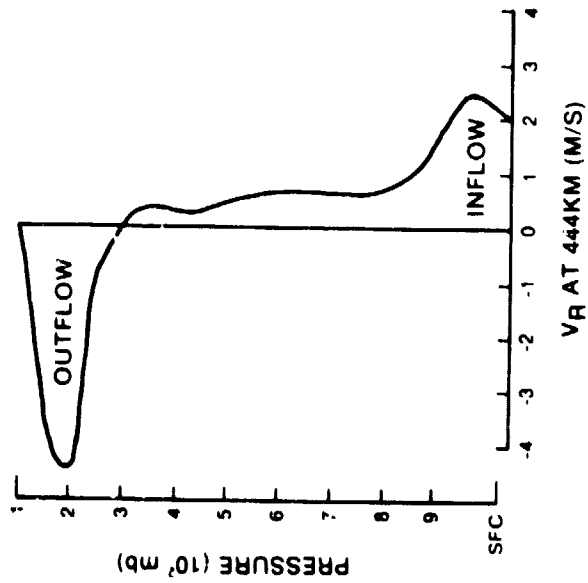
Figure 2. (a) mean radial wind profile derived from the composite rawinsonde data at 444 km radius from the center for the Western Atlantic hurricanes adapted from McBride (1979) (b) a simplified model of McBride's (1979) radial wind profile.

14

mass divergence was computed by adjusting the pressure height (P) at the top of the inflow so that the lower tropospheric areal mean mass convergence balanced the upper tropospheric areal mean mass divergence between 100 and 300 mb (see Fig. 2b). With these assumptions, the equation per unit area becomes:

$$\frac{\partial m}{\partial t} = \frac{2}{g}\left[\int_{1000\ mb}^{P}\overline{V_r V_t}\,dP + \frac{1}{2}\int_{300\ mb}^{100\ mb}\overline{V_r V_t}\,dP\right]$$

$$+ \frac{2}{g}\left[\int_{1000\ mb}^{P}\overline{fRV_r}\,dP + \frac{1}{2}\int_{300\ mb}^{100\ mb}\overline{fRV_r}\,dP\right] - 0.64\,C_D\rho|V|V_t R$$

(3)

where P is the upper limit pressure height of the low-level areal mean mass convergence that assures the lower tropospheric areal mean mass convergence balances the upper tropospheric areal mean mass divergence.

Table 2 shows the mean magnitude for each measured term in the equation for a cylindrical volume of radius 444 km and between the surface and 100 mb, with respect to cyclone intensity. These data were obtained from the 14 year composite of north Atlantic rawinsonde data that were partitioned for storm intensity (McBride, 1979).

TABLE 2

Relative Angular Momentum (10^4 kg s^{-2})

Intensity	$\overline{V_r V_t}$	$\overline{RfV_r}$	$C_D|V|V_t R$	$\partial m/\partial t$
Non-developing Depression	5.8	-2.8	-0.9	2.1
Pre-hurricane Cloud Cluster	10.6	-2.2	-1.0	7.4
Pre hurricane Depression	11.3	-2..	-1.7	7.5
Intensifying Cyclone	19.0	· 3.2	-2.4	13.4
Hurricane	11.7	-3.5	-5.2	3.0

This table shows that the largest values of the local change of relative angular momentum ($\partial m / \partial t$) occur with intensification rather than storm intensity itself. Frank (1977a) showed for 20 years of composite rawinsonde data of western Pacific typhoons at the radius of 333 km from the center of circulation (the same radius that was used in this study for calculating relative angular momentum balance) that the net mass transport, which has a mean magnitude of approximately 21×10^4 kg s^{-1}, was balanced primarily by frictional dissipation. The magnitude of the net coriolis torque for the column at this radius was small and negative (approximately -5×10^4 kg s^{-2}) causing spin-down of the storm. The effect of the coriolis torque at large radii, however, becomes greater. The magnitude of the individual terms of the balance of relative angular momentum calculations for the case studies were quite similar when compared to those found by Frank (1977a) and will be discussed in section 4.

c.   The Upper Tropospheric Mass Outflow

The importance of the upper tropospheric outflow has been evaluated by Sadler (1976). He found that developing and intensifying tropical cyclones in the western Pacific typically possessed two outflow channels, which were manifestations of the tropical upper tropospheric trough (TUTT). A similar phenomena has been observed in the Atlantic with only one predominant channel toward northeast of the storm. The physical reasoning for this is related to the enhancement of the inward transport of relative angular momentum. A stronger and more anticyclonic upper tropospheric outflow helps to "spin-up" the tropical cyclone system. Thus, the detection and monitoring of these outflow channels may aid in evaluating and predicting tropical cyclone formation and intensification.

To examine these upper tropospheric outflow channels, mass outflow was calculated for each quadrant. In deriving this parameter the average satellite-derived V_r was calculated for each quadrant after subtracting out the storm motion. The cirrus level was assumed to represent the maximum outflow in the layer between 300 to 100 mb (see Fig. 2). Thus, the mass outflow for each quadrant is:

$$\text{mass outflow} = \frac{1}{2g} \sum_{\text{Quadrant}} V_r \Delta P \tag{4}$$

where V_r obtained from cirrus tracers is averaged along a cylindrical surface at radius of 333 km from the center of circulation for each quadrant, P is the pressure height of the outflow layer, and g is gravity.

d. Upper-Tropospheric Subsidence

Arnold (1977) postulated that tropical cyclone formation may occur in regions where a lower tropospheric cyclone vortex is superimposed upon an area of dynamically forced upper tropospheric subsidence. This subsidence results from the convergence of the outflows from adjacent deep convective cells or between convective cells and the environment. The subsiding air causes warming through adiabatic compression which hydrostatically lowers the surface pressure within the column. The lower pressure enhances lower tropospheric mass and moisture convergence, thereby increasing the enthalpy of the column through both adiabatic warming and latent heat release from the enhanced convection. This enhanced convection initiates the release of Conditional Instability of the Second Kind (CISK) that is needed for further development. This sequence was observed in tropical cyclone Anita. The 3h time history of convective development associated with Anita, together with the environmental upper tropospheric horizontal divergence calculations and the upper and lower tropospheric wind analyses, will be shown in section 4b.

4. CASE STUDIES

a. Caroline

Caroline was first observed as a tropical disturbance off the African West Coast on August 15, 1975. It failed to strengthen until reaching the southwest Gulf of Mexico on August 28, when Air Force reconnaissance aircraft found winds of tropical storm strength (17 to 31 ms^{-1}) late that day. Caroline reached hurricane strength late on August 29 and intensified further at a very rapid rate.

On August 30 Caroline's maximum surface winds were approximately 50 ms^{-1} as it moved slowly (2.5 ms^{-1}) across the Gulf of Mexico towards landfall 185 km south of Brownsville, Texas. The central pressure fell from 987 mb at 1800 GMT on August 30 to 963 mb at 0600 GMT on August 31 (Hebert, 1976). Fig. 3 shows the central pressure and maximum wind history between August 28 to August 30, 1975. Arrows represent the times at which SMS-2 rapid-scan observations were made.

The main synoptic weather pattern that dominated during the time of the satellite observation was a lower tropospheric anticyclone over the southeastern states that kept Caroline in an easterly flow as it moved across the Gulf of Mexico. The upper tropospheric flow around Caroline was northeasterly. This flow was caused by a large anticyclone over Texas and Mexico, which was building into the western Gulf of Mexico. Figures 4a and b show a streamline analyses of the environmental lower and upper tropospheric wind field for 0000 GMT on August 30, which depicts the synoptic patterns during that period. The streamline analyses were derived from the 850 and 200 mb rawinsonde data along with satellite-derived winds (not shown) that were extrapolated to the rawinsonde time. Figures 5a and b show the satellite-derived winds for 1600 GMT on August 29 used to deduce the lower and upper tropospheric streamline analyses and the kinematic parameters.

The kinematic parameters for the satellite observation times for Caroline are seen in Tables 3, 4, and 5 which respectively show the areal mean relative vorticity for the lower and upper troposphere and vertical difference, the relative angular momentum balance, and the upper tropospheric mass flow for each quadrant. The areal mean relative vorticity and mass flow were computed at a radius of 333 km from Caroline's center. The relative angular momentum was computed for a cylindrical volume of 333 km radius from the center of the cyclone with a depth from the surface to 100 mb.

TABLE 3

Areal Mean Relative Vorticity (10^{-5} s^{-1})

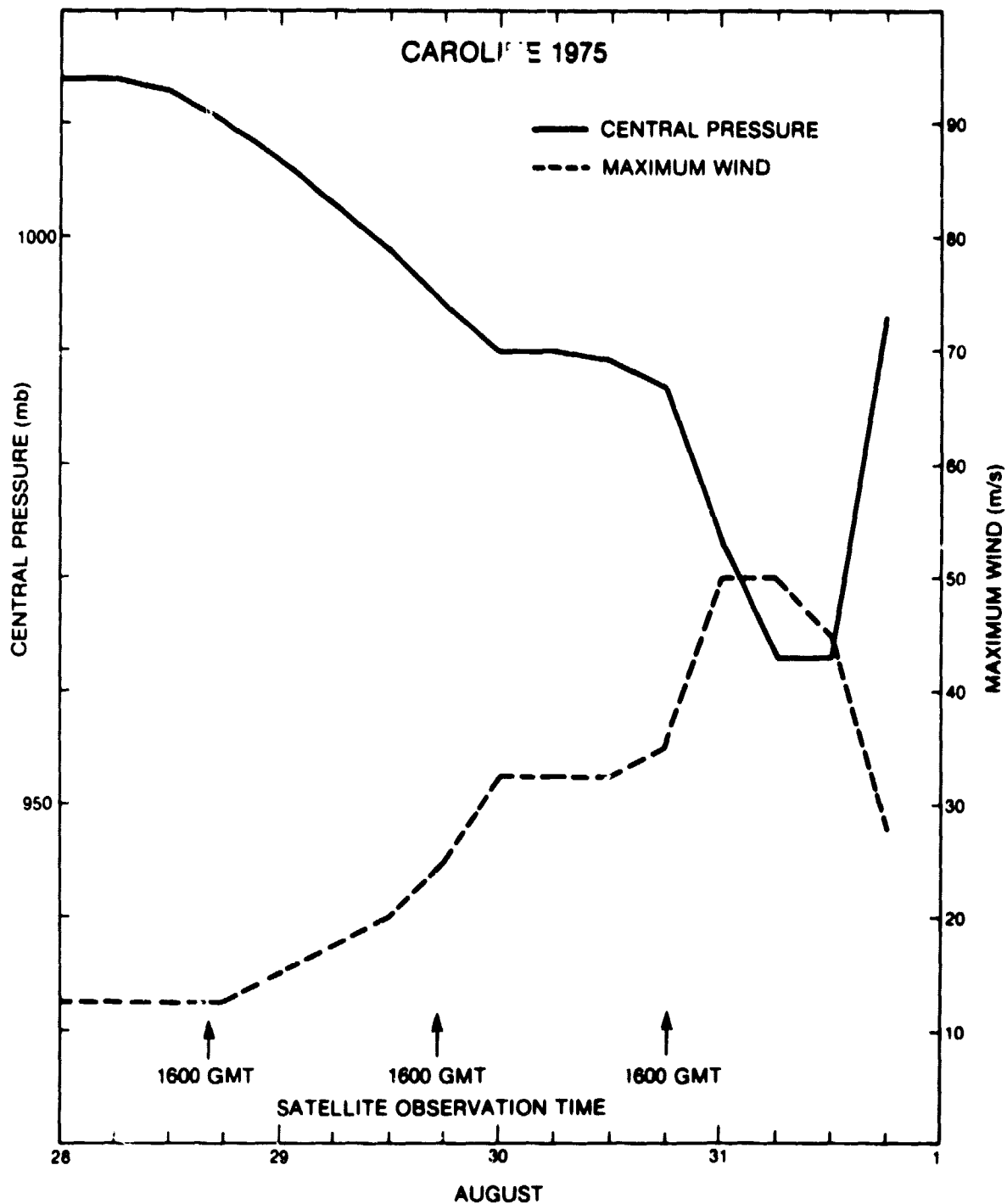| Time	Cloud Base Level	Cirrus Level	Vertical Difference
Aug. 28 1600 GMT	3.7	−2.5	6.2
Aug. 29 1600 GMT	5.6	1.3	4.3
Aug. 30 1600 GMT	4.8	−1.6	6.4

Figure 3. Time history of tropical cyclone Caroline's maximum winds (dashed) and central pressure (solid) during the period of 28 August to 1 September, 1975. Arrows indicate time of satellite observations.

TABLE 4

Relative Angular Momentum (10^4 kg s^{-2})

Time	Cloud Base Level $\overline{V_r V_t}$	Cirrus Level $\overline{V_r V_t}$	Net $\overline{V_r V_t}$	Cloud Base Level $\overline{fV_r R}$	Cirrus Level $\overline{fV_r R}$	Net $\overline{fV_r R}$	$\rho C_D V_t R$	$\dfrac{\partial m}{\partial t}$
Aug. 28 1600 GMT	7.6	4.8	12.4	7.2	−6.6	0.6	−1.1	11.9
Aug. 29 1600 GMT	6.9	0.9	7.8	6.6	−6.5	0.1	−3.2	3.8
Aug. 30 1600 GMT	14.7	3.5	18.2	16.1	16.5	−0.4	−2.4	15.4

TABLE 5

Rate of Mass Flow at the Cirrus Level (10^{-3} mb s^{-1})

Time	NE	SE	SW	NW
Aug. 28 1600 GMT	−5.7	−4.3	−2.4	2.5
Aug. 29 1600 GMT	−3.6	0.9	−4.2	1.4
Aug. 30 1600 GMT	−6.2	−2.7	−5.3	−6.0

Comparing the results from these tables with Fig. 3, there appears to be a relationship between the effects of the environmental circulation surrounding Caroline and its future change in intensity. The magnitude of the vertical difference in areal mean relative vorticity (Table 3), although somewhat smaller than that expected from McBride's (1979) composite model (Table 1) for either an intensifying tropical cyclone or a hurricane, appeared to be related to future changes in storm intensity. The vertical difference of areal mean relative vorticity decreased in magnitude prior to the time when Caroline became a steady state storm early on August 30 and then increased prior to Caroline's rapid development later that day[1]. The decrease in magnitude of this parameter was mainly in response to

---

[1] The smaller magnitude of the areal mean relative vorticity calculations may be attributed to assuming that the storm's maximum outflow is at the cirrus level.
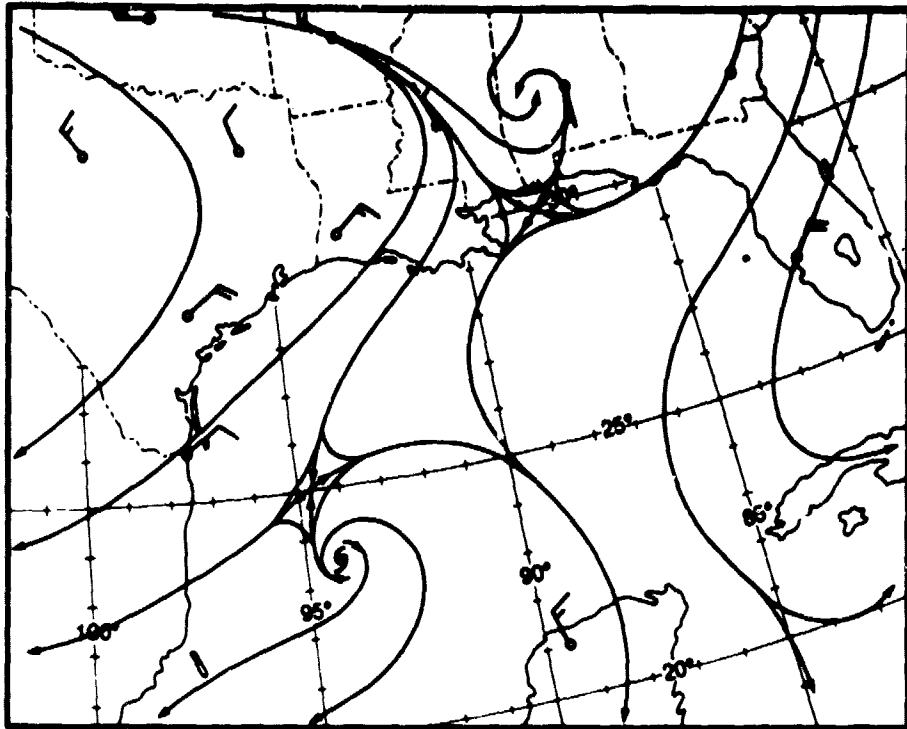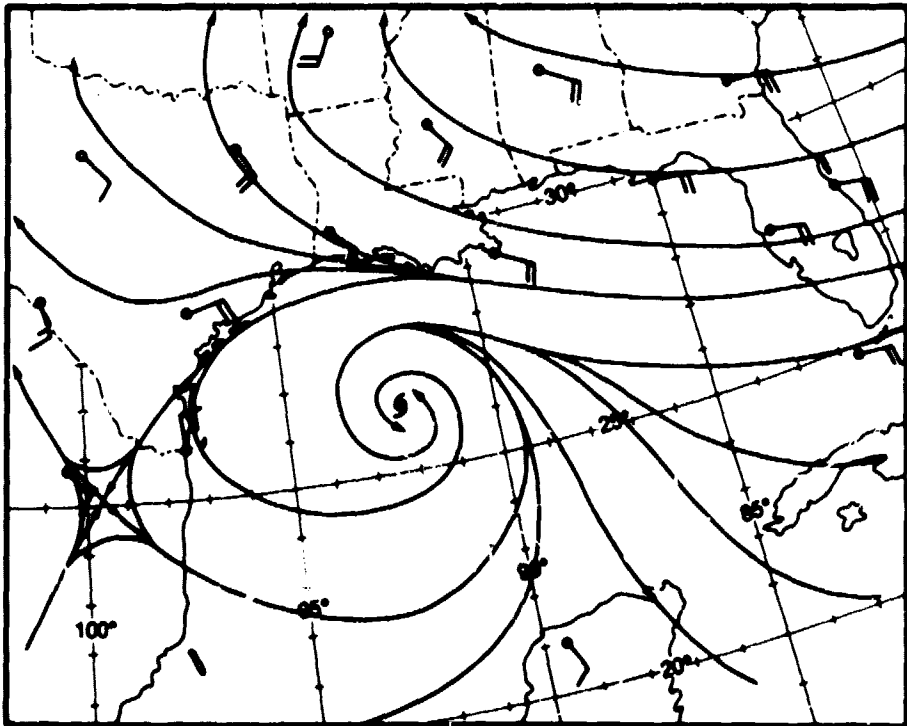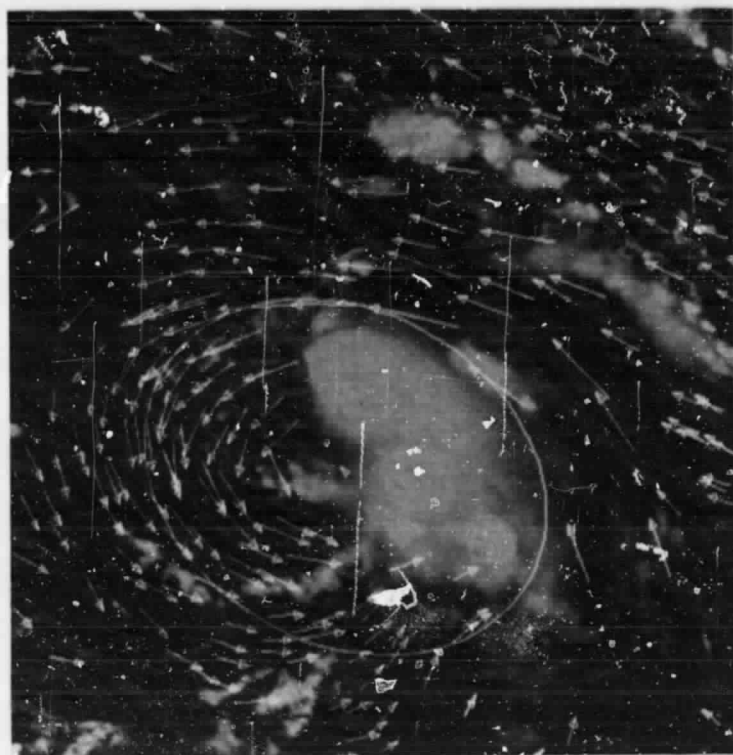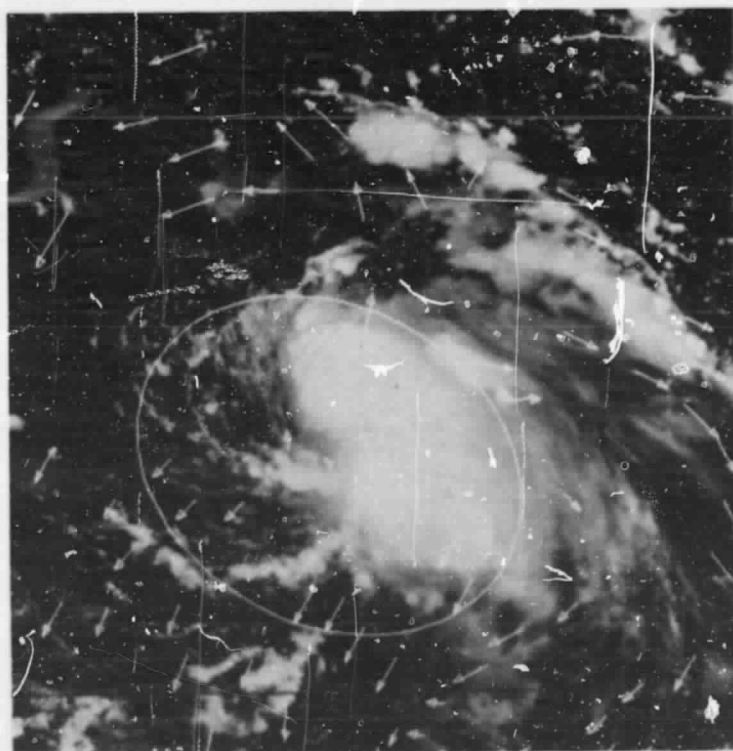
Figure 4. Streamline analyses of tropical-cyclone Caroline's (a) lower and (b) upper tropospheric environmental wind field derived from 0000 GMT 30 August 1975 observed 850 and 200 mb rawinsonde data, respectively, together with the satellite-derived winds (not shown) that were extrapolated to the rawinsonde time. Wind speed in knots.

(a)

(b)

Figure 5. SMS-2 derived winds of tropical cyclone Caroline at
the (a) cumulus cloud base and (b) cirrus level at 1600 GMT
29 August, 1975. Otherwise the same notation as in Figure 1a.

the interaction between the outflow and the upper tropospheric anticyclonic circulation over Mexico. This interaction produced cyclonic flow west of the storm, which yielded an areal mean cyclonic vorticity of 1.3×10^{-5} s^{-1} at 1600 GMT on August 29.

The magnitude of the local change of relative angular momentum (Table 4) also exhibited this lag relationship. A dramatic decrease in relative angular momentum on August 29 preceded the steady state condition of Caroline earlier on August 30. This decrease was mainly in response to the decrease in the upper tropospheric horizontal transport of relative angular momentum and, to a lesser degree, to an increase in frictional dissipation. The decrease in the upper tropospheric horizontal relative angular momentum was caused by horizontal divergence of cyclonic vorticity south-west of the storm. This occurred in response to the influence of the northerly flow produced by the upper tropospheric anticyclone over Mexico. At 1600 GMT on August 30, the dramatic increase of the local change of relative angular momentum preceded rapid intensification. This change was mainly caused by the large increase of convergence of cyclonic vorticity at the cumulus cloud base level and to a lesser extent to a large increase of divergence of weak anticyclonic vorticity at the cirrus level.

The magnitude of mass flow (Table 5) indicates that all quadrants at the last satellite observation time (1600 GMT on August 30) are depicting mass outflow with a particularly strong outflow channel to the north of the storm. The strong outflow channel in the northwest quadrant developed during the last 24h period and may have been partially responsible for the onset of rapid intensification.

b.   Anita

Anita originated off the African coast on August 16, 1977, as a tropical disturbance. She maintained this status while moving across the Atlantic, Caribbean, and into the Gulf of Mexico on August 28. On August 29, while Anita was in the eastern Gulf of Mexico, she was upgraded to a tropical depression. As Anita moved west-southwestward towards the Mexican coast, she intensified rapidly from tropical storm stage at 0600 GMT on August 30 to a hurricane at 1800 GMT on the same day. Anita continued to intensify reaching a minimum pressure of 926 mb (75 ms^{-1} maximum

23

winds) just prior to landfall as her forward speed accelerated from 2 ms^{-1} to 10 ms^{-1}. During her traverse across the Gulf of Mexico, Anita intensified over warm waters within an atmosphere that was warm and moist (Lawrence, 1978). Fig. 6 shows Anita's central pressure and maximum wind history between August 30 and September 3, 1977. Arrows again indicate the times at which GOES-1 rapid-scan observations were made.

The synoptic scale upper and lower tropospheric patterns during the time of the satellite observations of Anita were similar to those associated with Caroline. Over the southeastern United States, a large lower tropospheric anticyclone persisted during the 3 days, while at the upper tropospheric level, a large anticyclone west of Anita caused north to northeasterly flow. The combination of this upper tropospheric flow, together with Anita's outflow, caused a very intense jet southeast of Anita. Figures 7a and b show streamline analyses of the 850 and 200 mb wind flow at 1200 GMT on August 31 depicting the environmental circulation. These streamline analyses were again constructed from rawinsonde data and satellite-derived wind data (not shown) that was extrapolated to 1200 GMT. Figures 8a and b show the satellite-derived winds for 1600 GMT on August 31 at the cloud base and cirrus levels that contributed to the streamline and kinematic analyses.

On August 30 rapid-scan images were available during the time of Anita's rapid transition from a depression to a tropical storm. It appeared from the satellite images and derived kinematic parameters that Anita's lower tropospheric vortex rapidly developed in the region of upper tropospheric forced subsidence as postulated by Arnold (1977). Satellite-derived winds at 1300 GMT at the cloud base level (Fig. 9) delineated a vortex just west of the convective system associated with the wave. The dot represents the center of the vortex. At the same time, horizontal divergence patterns (Fig. 11) depicted a region of upper tropospheric confluence (dashed lines) superimposed upon the lower tropospheric cyclonic vortex. This area of confluence occurs in response to the convergence of the outflow from the convective system with the basic current. This confluence area is also delineated by satellite-derived winds at the cirrus level (Figures 10, 12 and 13). Since there is no upper and middle tropospheric cloud cover over the vortex and there is a strong demarcation
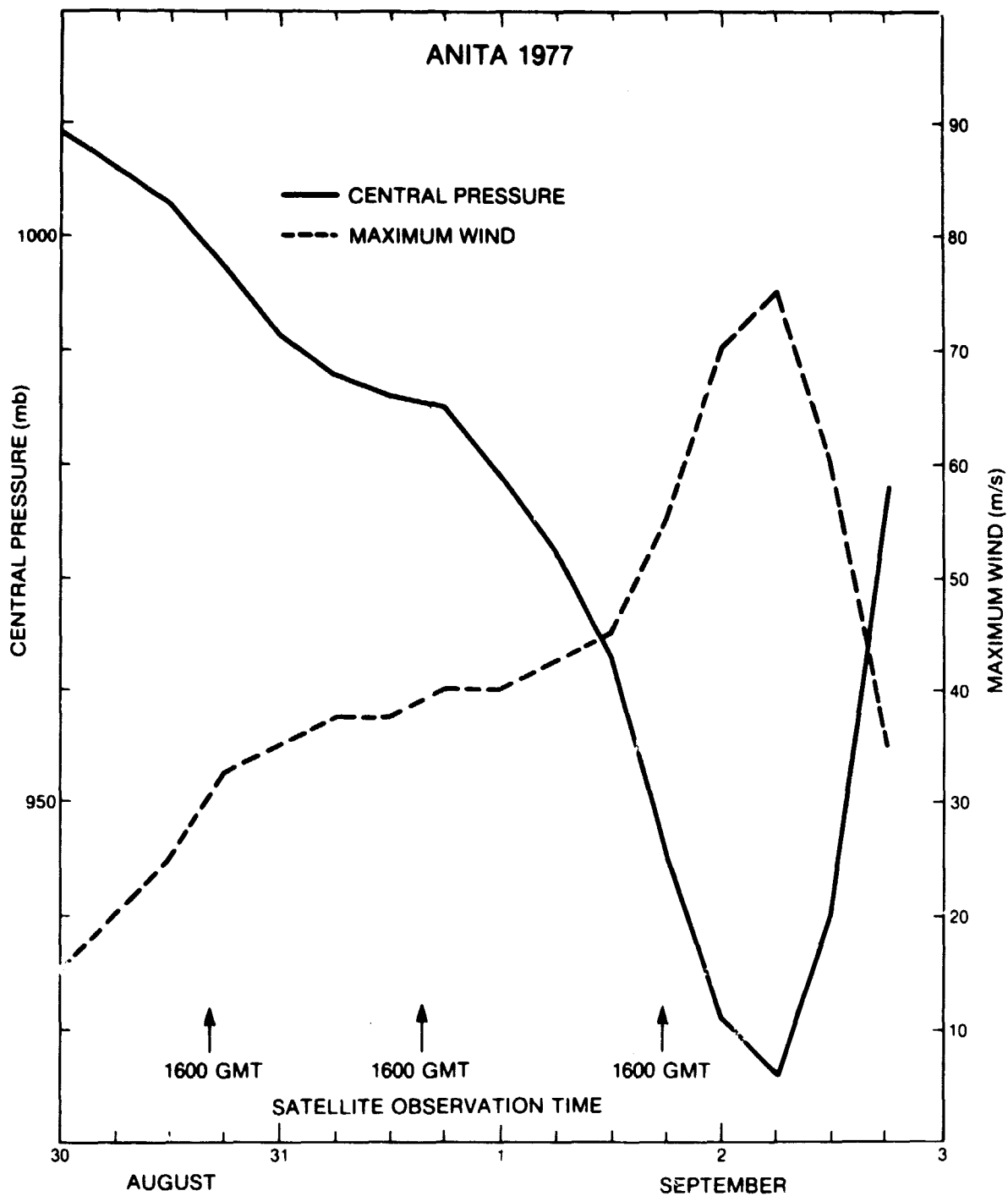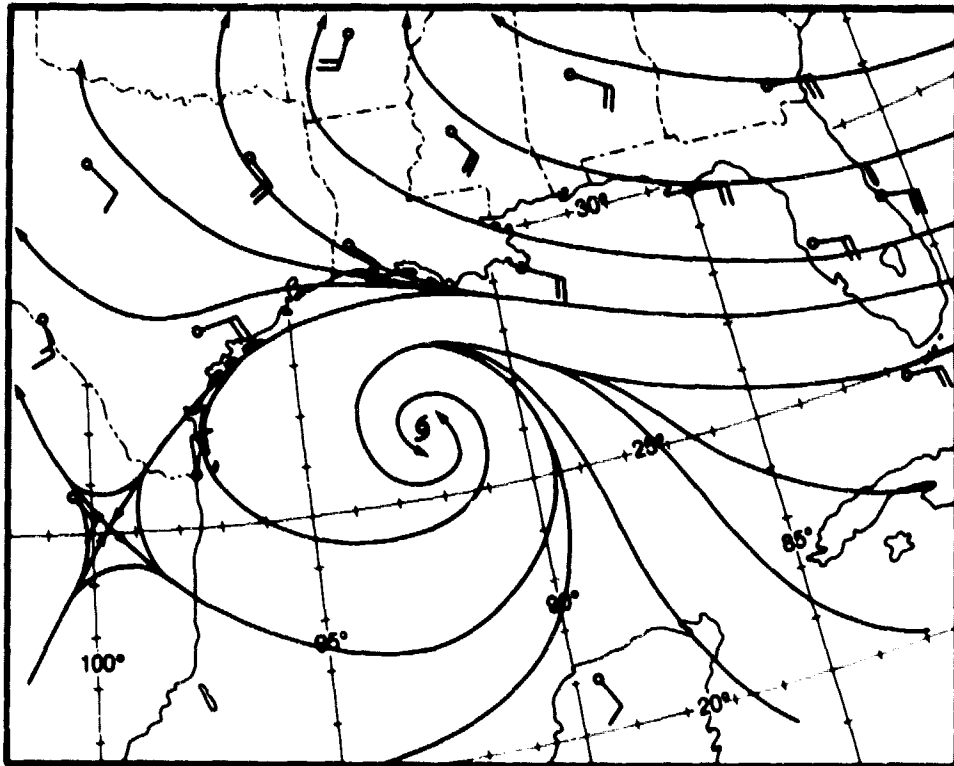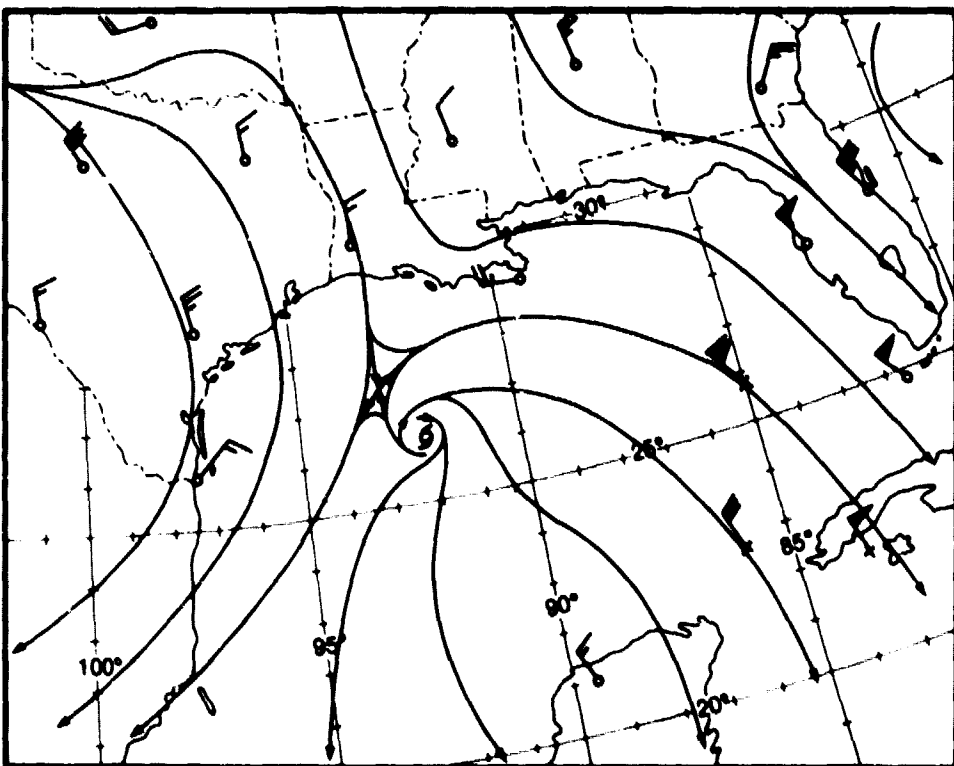
24

Figure 6. Time history of tropical cyclone Anita's maximum winds and central pressure for the period 30 August to 3 September, 1977. Otherwise the notation is the same as in Figure 3.
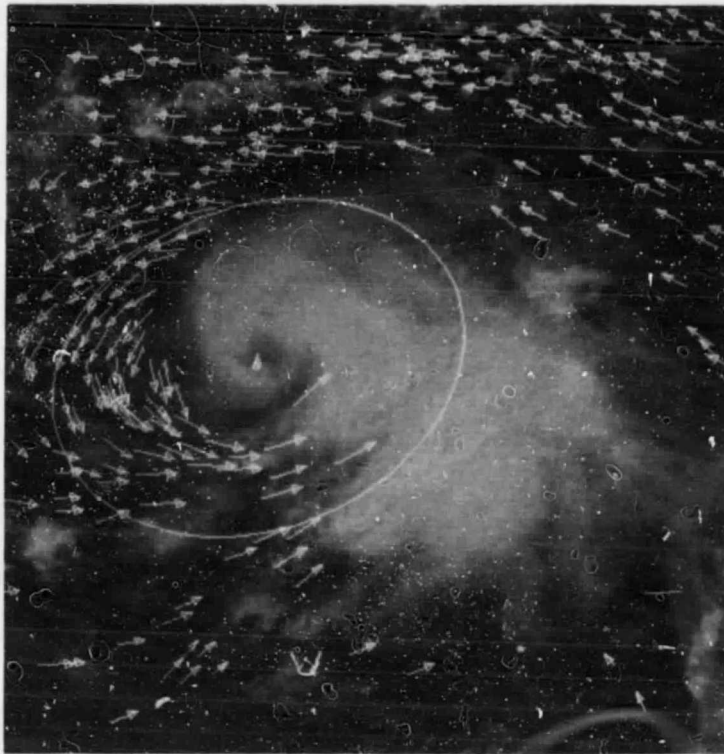
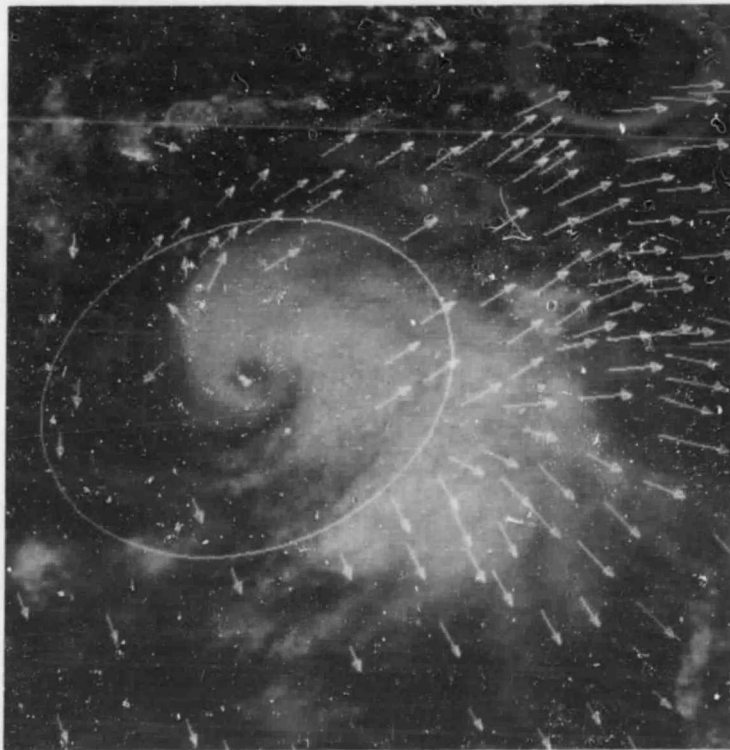Figure 7. Streamline analyses of tropical cyclone Anita's (a) lower and (b) upper tropospheric environmental wind field at 1200 GMT 31 August, 1977. Otherwise the notation is the same as in Figure 4.

(a)

(b)

Figure 8. GOES-1 derived winds of tropical cyclone Anita's (a) lower
and (b) upper tropospheric environment at 1600 GMT 31 August,
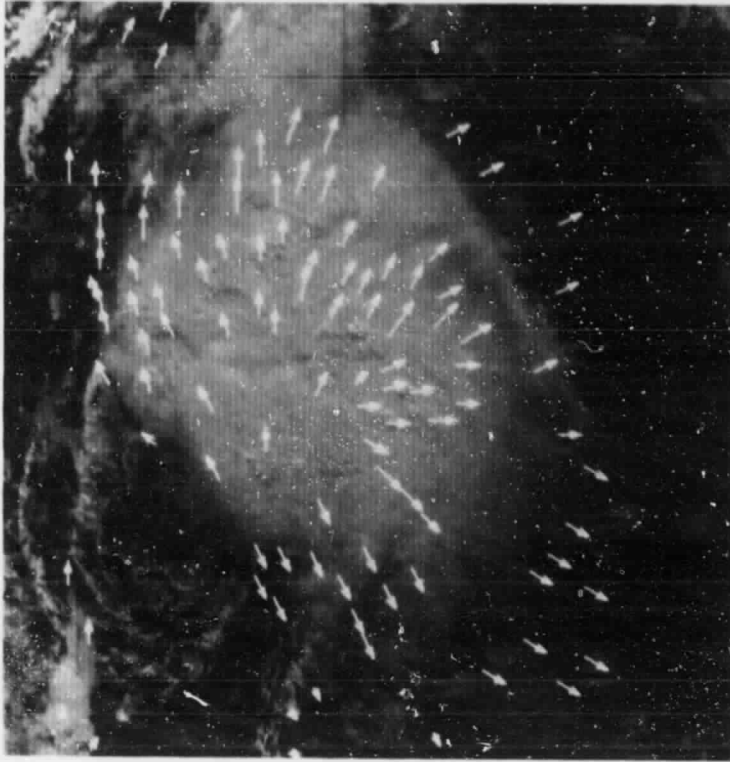1977. Otherwise the notation is the same as in Figure 1a.

Figure 10. GOES-1 derived winds at the cirrus level for cyclone Anita 1300 GMT 30 August, 1977. Otherwise notation is the same as in Figure 1a.

Figure 9. GOES-1 derived winds at the cumulus cloud base level for tropical cyclone Anita 1300 GMT 30 August, 1977. Dot represents the center of lower tropospheric circulation. Otherwise notation same as in Figure 1a.

Figure 12. GOES-1 derived winds at the cirrus level for tropical cyclone Anita 1600 GMT 30 August, 1977. Otherwise notation is the same as in Figure 1a.

Figure 11. Horizontal divergence field calculated from GOES-1 derived winds at the cirrus level for tropical cyclone Anita 1300 GMT 30 August, 1977. Dashed (solid) lines represent horizontal convergence (divergence). Otherwise notation is the same as in Figure 1a.

Figure 13. GOES-1 derived winds at the cirrus level for tropical cyclone Anita 1900 GMT
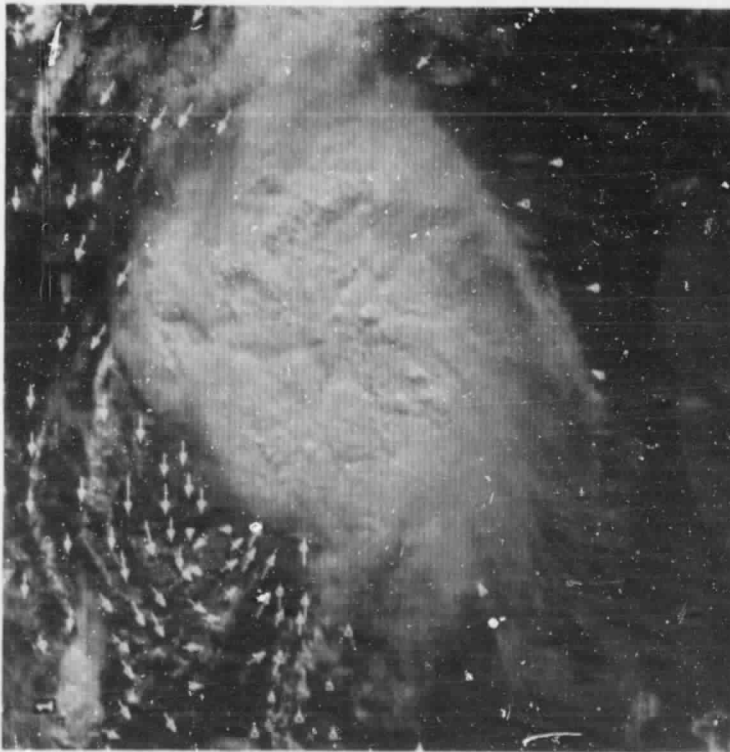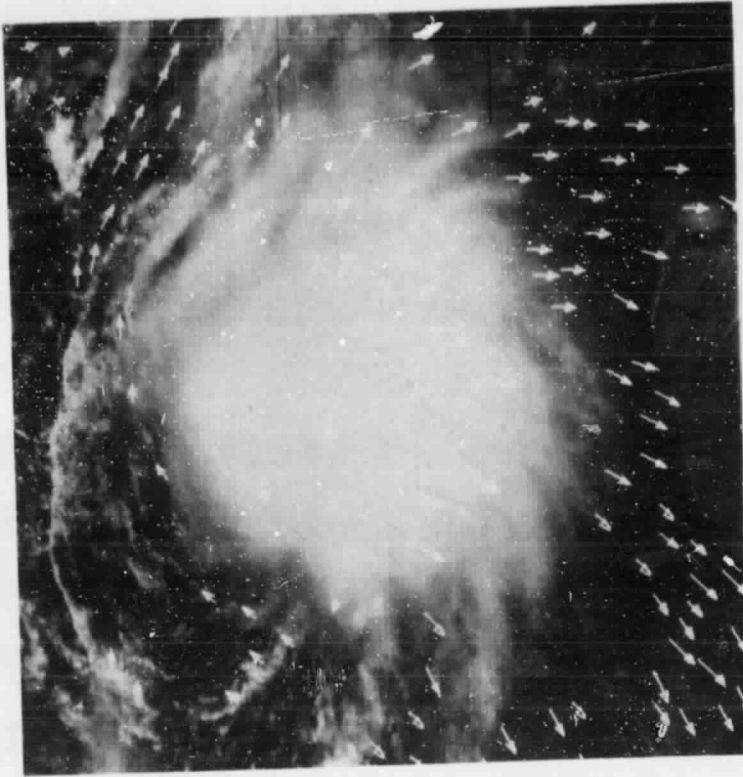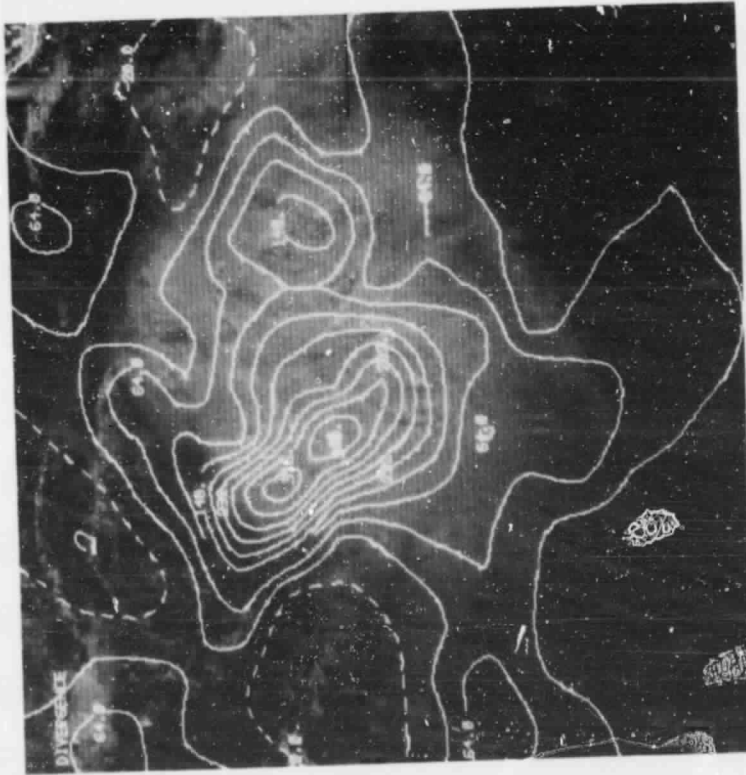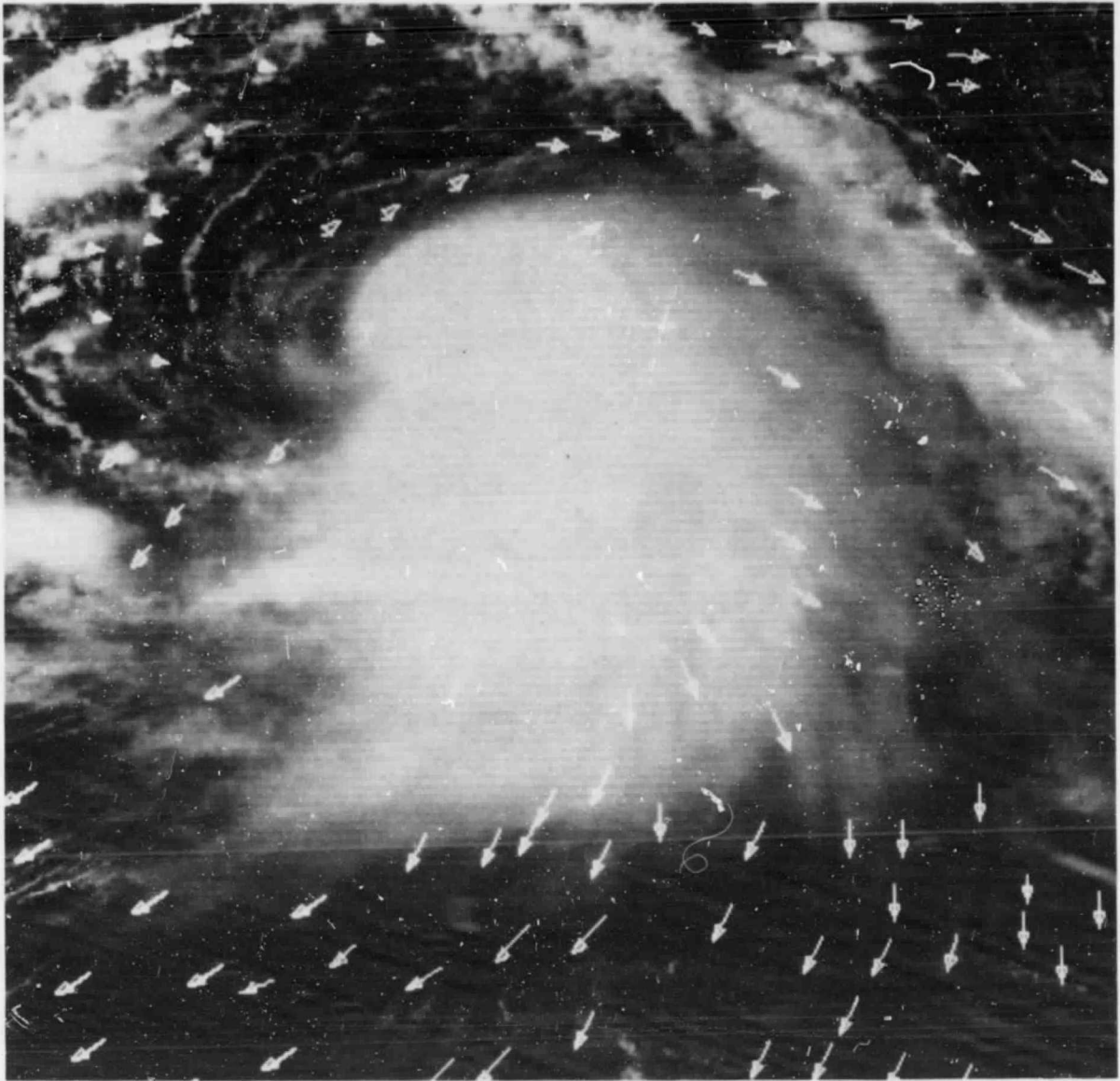30 August, 1977. Otherwise notation is the same as in Figure 1a.

between the cirrus and the clear area west of the convective systems, it is assumed that the upper tropospheric confluence is producing subsidence down to the middle troposphere. Figures 10, 12 and 13 also show Anita's cloud systems with the cirrus level wind arrows superimposed at 1300, 1600 and 1900 GMT on August 30. It appears from these figures that the convection is rapidly developing within the lower tropospheric vortex. Approximately 24h later figures 8a and b show the transition of the cloud systems from an open cyclonic vortex to one with a deep convective ring with an eye at 1600 GMT on August 31. At this time, Anita was at the tropical storm stage and developing rapidly (see Figure 6).

The kinematic parameters derived for the satellite observation times in Fig. 6 are seen in Tables 6, 7 and 8. These tables are similar to Tables 3, 4 and 5, respectively.

TABLE 6

Areal Mean Relative Vorticity (10^{-5} s^{-1})

Time	Cloud Base Level	Cirrus Level	Vertical Difference
Aug. 30 1600 GMT	6.3	–4.3	10.6
Aug. 31 1600 GMT	6.8	0.7	6.1
Sept. 1 1600 GMT	9.9	–1.8	11.7

TABLE 7

Relative Angular Momentum (10^4 kg s^{-2})

Time	Cloud Base Level $\overline{V_r V_t}$	Cirrus Level $\overline{V_r V_t}$	Net $\overline{V_r V_t}$	Cloud Base Level $\overline{rV_r R}$	Cirrus Level $\overline{rV_r R}$	Net $\overline{rV_r R}$	$\rho C_D|V|V_t R$	$\dfrac{\partial m}{\partial t}$
Aug. 30 1600 GMT	17.5	11.5	29.0	19.0	–19.0	0	–4.3	24.7
Aug. 31 1600 GMT	18.8	1.7	20.5	15.8	–16.4	–0.6	–4.7	15.2
Sept. 1 1600 GMT	22.8	9.5	32.3	13.9	–12.7	1.2	9.9	23.6

TABLE 8

Rate of Mass Flow at Cirrus Level (10^{-3} mb s^{-1})

Time	NE	SE	SW	NW
Aug. 30 1600 GMT	-5.1	-12.3	-5.8	1.9
Aug. 31 1600 GMT	-8.9	-7.5	-1.1	1.5
Sept. 1 1600 GMT	-5.0	-5.7	-6.1	2.1

Comparing these results from these tables with Fig. 6, a relationship again appears between future changes in tropical cyclone intensity and the environmental circulation at 333 km radius from the center. The vertical differences of areal mean relative vorticity are much larger than were measured with Caroline. This is a reasonable result, since Anita was a more intense storm with values slightly exceeding the composite values for hurricanes at approximately the same radius (see Table 1). The decrease in the vertical difference of relative vorticity at 1600 GMT on August 31, seems to be related to the decrease in Anita's intensity. This is mainly caused by an abrupt reversal of areal mean relative vorticity from anticyclonic to cyclonic at the upper tropospheric level in response to the northerly flow west of Anita. This northerly flow was caused by the upper tropospheric anticyclone over the southwestern United States. At the cloud base level, however, the cyclonic vorticity continued to increase. During rapid intensification on 1 September, the cloud base areal mean cyclonic relative vorticity increased dramatically. Also, at the upper tropospheric level the areal mean relative vorticity became anticyclonic again. These changes in the areal mean relative vorticity at the two levels helped to increase the magnitude of the vertical difference.

The magnitude of the local change in relative angular momentum (Table 7) for Anita, which also showed larger magnitudes than Caroline's, reflected Anita's decrease in the intensification rate on August 31. This is attributed mainly to an abrupt decrease in the inward horizontal transport of upper tropospheric relative angular momentum caused by the convergence of anticyclonic vorticity in the southwest quadrant. However, similar to Caroline, the upper

tropospheric mass convergence in the NW quadrant (Table 8) was transporting cyclonic vorticity radially inward, thus increasing the "spin-up" of Anita's circulation. During the time of rapid development on September 1, the local change of relative angular momentum once again increased, but only to the magnitude measured on August 30. This change was caused by the increase of the inward horizontal transport of relative angular momentum in both the lower and upper troposphere. The reason that the local change of relative angular momentum was not greater was because of the nearly 100 percent increase in surface frictional dissipation.

The upper tropospheric mass outflow (Table 8) shows that during the slowing of Anita's intensification rate on August 31, the mass outflow in the southwest quadrant decreased considerably under the influence of the upper tropospheric anticyclonic flow west of Anita. The outflow in the southeast quadrant also decreased. During Anita's rapid intensification on September 1, the upper tropospheric outflow continued to decrease in the southeast quadrant, but dramatically increased in the southwest quadrant. This increasing southwest outflow channel may have been partially responsible for Anita's rapid intensification. Throughout the period, the upper tropospheric anti-cyclone west of Anita prevented an outflow channel in Anita's northwest quadrant.

c.   Ella

Ella originated on a quasi-stationary frontal zone over the central North Atlantic Ocean on August 28, 1978, and became a depression at 0000 GMT on August 30. As a depression, Ella moved west-northwest at 5-8 ms^{-1} toward the United States, intensifying to storm stage on August 30. As it moved toward the North Carolina coast, it intensified to hurricane strength at 1800 GMT on August 31. During the times of the satellite observations on September 1-3, Ella interacted with two short-wave middle and upper level troughs that affected the cyclone. The first trough passed to the north of Ella causing her to decelerate and weaken on September 2. The second trough caused Ella to rapidly intensify and accelerate toward the northeast at speeds close to 9 ms^{-1} on September 3 (Lawrence, 1979). Figure 14 shows the central pressure and the maximum wind history between September 1-3, 1978. Arrows again depict the times of the satellite rapid-scan observations that
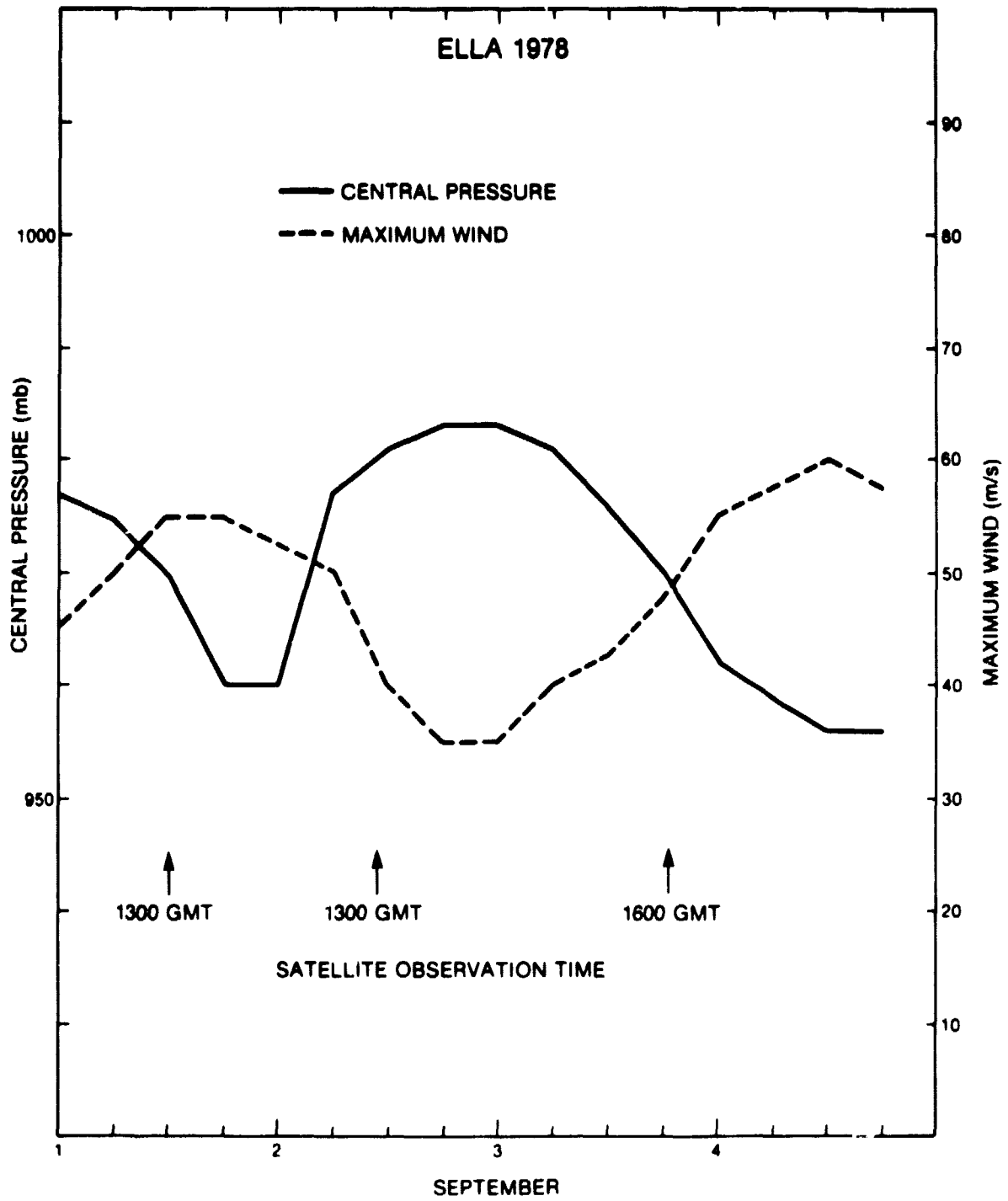
33

Figure 14. Time history of tropical cyclone Ella's maximum winds and central pressure during the period of 1-4 September, 1978. Otherwise notation is the same as in Figure 3.

were used for the kinematic analysis.

The synoptic upper and lower tropospheric features affecting Ella during the period of satellite observations were the two previously mentioned middle and upper level troughs. In the lower troposphere, a stationary front stayed northwest of Ella while southeasterly flow into the southeastern sector dominated during the 3-day period. In the upper troposphere, the first trough moving from the west and passing north of Ella acted as a barrier to Ella's outflow toward the west. However, the second trough, which had greater amplitude, enhanced Ella's outflow. Figures 15a and b show streamline analyses of the 850 and 200 mb winds at 1200 GMT on September 2, 1978 and depict the lower and upper tropospheric circulation during the time of Ella's interaction with the first trough. These streamline analyses were constructed from the rawinsonde data and satellite-derived wind data (not shown) were extrapolated to 1200 GMT. Figures 16a and b show the satellite-derived winds at the cloud base and cirrus levels for 1600 GMT on September 2 that were used in the streamline and kinematic analyses.

The kinematic parameters for satellite observation times for Ella as depicted by the arrows in Fig. 14 are seen in Tables 9, 10, and 11. These tables are similar to Tables 3, 4, and 5, respectively.

TABLE 9

Areal Mean Relative Vorticity (10^{-5} s^{-1})

Time	Cloud Base Level	Cirrus Level	Vertical Difference
Sept. 1 1300 GMT	3.6	-4.3	7.9
Sept. 2 1300 GMT	4.9	-2.2	7.1
Sept. 3 1300 GMT	7.5	-0.8	8.3
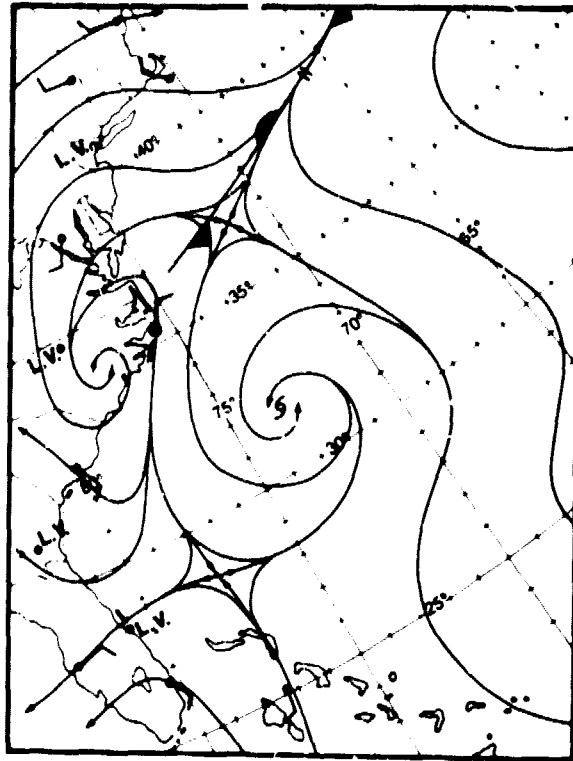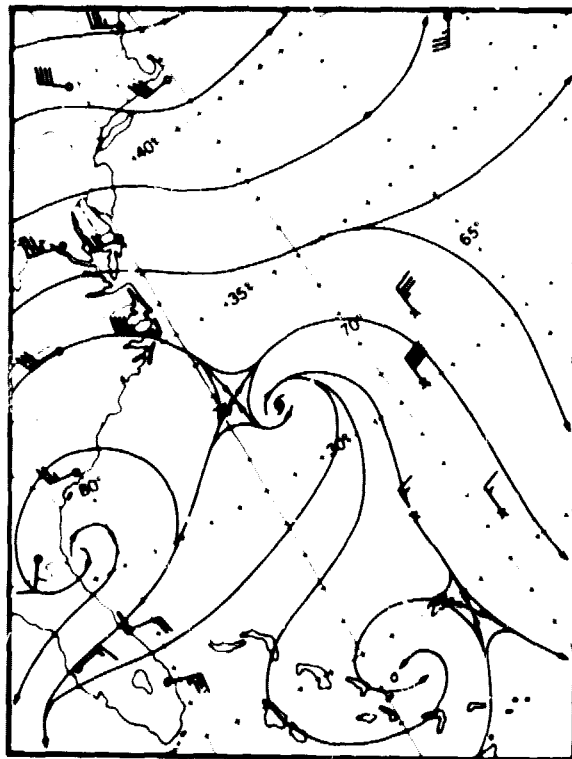
Figure 15. Streamline analysis of tropical cyclone Ella's (a) lower and (b) upper tropospheric environmental wind field at 1200 GMT 2 September, 1978. Otherwise notation is the same as in Figure 4.

36

(a)

(b)

Figure 16. GOES-1 wind of tropical cyclone Ella at the (a) cumulus cloud base and (b) cirrus level at 1600 GMT 2 September, 1978. Otherwise notation is the same as in Figure 1a.

37

TABLE 10

Relative Angular Momentum (10^4 kg s^{-2})

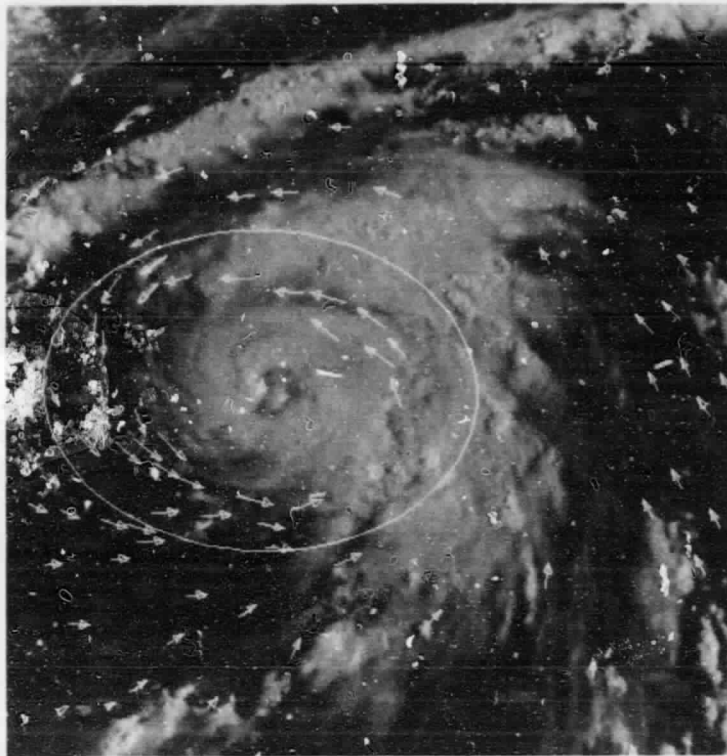| Time	Cloud Base Level $\overline{V_r V_t}$	Cirrus Level $\overline{V_r V_t}$	Net $\overline{V_r V_t}$	Cloud Base Level $\overline{fV_r R}$	Cirrus Level $\overline{fV_r R}$	Net $\overline{fV_r R}$	$\rho C_D |V|V_t R$	$\frac{\partial m}{\partial t}$
Sept. 1 1300 GMT	8.9	11.5	20.4	18.0	-17.7	0.1	-1.3	19.2
Sept. 2 1300 GMT	11.2	7.2	18.8	17.1	-15.1	2.0	-2.6	18.2
Sept. 3 1300 GMT	27.6	3.2	30.8	32.1	-29.2	0.9	-5.8	25.9

TABLE 11

Rate of Mass Flow at the Cirrus Level (10^{-3} mb s^{-1})

Time	NE	SE	SW	NW
Sept. 1 1300 GMT	-3.4	-4.9	-5.0	-3.9
Sept. 2 1300 GMT	-3.3	-7.0	-6.9	2.2
Sept. 3 1300 GMT	-6.5	-3.8	-6.0	-7.2

Comparing results from these tables with Fig. 14, there again appears to be a relationship between the environmental circulations and future changes in tropical cyclone intensity. At the 333 km radius from Ella's center, the vertical difference of areal mean vorticity (Table 9), which contains magnitudes approximately equal to that of the composite hurricane (Table 1), reflects Ella's weakening on September 2 and intensification on September 3. The weakening of this parameter was mainly caused by the increase in the upper tropospheric cyclonic vorticity in the south-western quadrant that reflected interaction of the first trough with Ella's outflow. The trough induced a strong northerly flow west of Ella at 333 km distance from the center. This was the same synoptic flow that affected both Caroline and Anita. Table 9 shows that the upper tropospheric

areal mean anticyclonic vorticity on September 3 continued to decrease even though Ella intensified. The intensification is reflected mainly in the increase of lower tropospheric areal mean relative cyclonic vorticity.

The magnitude of the local change of relative angular momentum (Table 10) indicates how the areal mean relative vorticity fields are affecting Ella's "spin-up" and, therefore, intensification. This parameter is again reflecting future changes in tropical cyclone intensity. These changes are mainly caused by the difference in horizontal transport although the surface frictional dissipation becomes more important as Ella intensifies. During the 3-day period, the lower tropospheric convergence of cyclonic vorticity increased as the upper tropospheric divergence of anticyclonic vorticity decreased. Although the lower tropospheric inward transport of relative angular momentum continued to increase, the interaction of the first trough with Ella's outflow decreased the gain of relative angular momentum due both to convergence of anticyclonic vorticity in the northwest quadrant and to the divergence of cyclonic vorticity in the southwest quadrant. Similar to tropical cyclone Caroline and Anita, Ella's intensification on September 3 is mainly attributed to the dramatic gain of relative angular momentum at the lower tropospheric level. However, unlike tropical cyclone Caroline and Anita, the enhancement of Ella's upper tropospheric outflow caused by the second trough did not increase the relative angular momentum at the cirrus level. This was attributed to the continuing deintensification of the areal mean anticyclonic vorticity (see Table 9). Therefore, it appears that the upper tropospheric outer circulation contributed little to Ella's intensification.

The upper tropospheric mass flow shown in Table 11 reflects the effects exerted by the two troughs on Ella's outflow. The first trough on September 2 completely blocked Ella's outflow in the northwest quadrant, causing horizontal convergence at 333 km radius as Ella moved into the convergent part of the upper tropospheric trough. As the second trough approached Ella, the storm moved into the divergent part of the trough, which enhanced the outflow in the northern part of the storm. However, as mentioned previously the rapid intensification of this outflow channel did not increase the magnitude of relative angular momentum because of the weakening of the upper tropospheric areal mean anticyclonic vorticity.

39

5. CONCLUSION

These three case studies indicate that satellite-derived lower and upper tropospheric kinematic analyses of the environmental circulations at 333 km radius from the storm's center can be used to monitor and possibly predict tropical cyclone formation and intensity changes. These kinematic analyses show that future changes in tropical cyclone intensity are mainly related to the "spin-up" of the storms by the net horizontal transport of relative angular momentum due to lower tropospheric convergence of cyclonic vorticity and to a lesser extent to the upper tropospheric divergence of anticyclonic vorticity. For these three tropical cyclones, the upper tropospheric environmental circulation helped to indicate the changes in intensity of these storms by hindering or enhancing the outflow. Major blocking of the outflow caused weakening in the case of Ella and slowed the intensification rates of Caroline and Anita. The strengthening of the outflow channels for Anita and Caroline helped to intensify the storms through the inward transport of relative angular momentum. The Anita case study suggested that satellite-derived wind fields can be used to ascertain whether tropical cyclone formation will occur if an area of concentrated upper tropospheric convergence is superimposed upon a lower tropospheric cyclonic vortex.

Thus, it appears from the three case studies that if the lower and upper tropospheric circulations surrounding a tropical cyclone are adequately defined, tropical cyclone formation and intensification can be monitored and possibly predicted. However, to adequately define these wind fields, full resolution rapid-scan geosynchronous satellite visible imagery must be used. Since the current SMS/GOES VISSR infrared channel has lower spatial resolution (approximately 8 km) these wind analyses can only be obtained during the day. Thus, the resolution of the infrared channel must be improved to approximately 1 km for similar results at night. To ascertain the lag time between the changes in the environmental circulation surrounding a storm and the storm's inner core characteristics (i.e., surface pressure, maximum winds) rapid-scan observation sequences are needed every few hours during the day and night.

REFERENCES

Adler, R. F. and E. B. Rodgers, 1977: Satellite-observed latent heat release in a tropical cyclone. Mon. Wea. Rev., 105, 956-963.

Arnold, C. P., 1977: Tropical cyclone cloud and intensity relationships. Atmos. Sc. Paper No. 277, Colorado State University, 154 pp.

Black, P. G., and R. A. Anthes, 1971: On the asymmetric structure of the tropical cyclone outflow layer. Mon. Wea. Rev., 99, 1348-1366.

Cressman, G. P., 1959: An operational objective analysis system. Mon. Wea. Rev., 87, 367-374.

Dvorak, V. R., 1975: Tropical cyclone intensity analysis system. Mon. Wea. Rev., 103, 420-430.

Erickson, S. L., 1977: Comparison of developing vs. non-developing tropical disturbances. Atmos. Sc. Paper No. 274, Colorado State University, 81 pp.

Erickson, C. O., 1974: Use of geostationary satellite cloud vectors to estimate tropical cyclone intensity. NOAA Tech. Memo, NESS 59, 37 pp.

Frank, W. M., 1977a: The structure and energetics of the tropical cyclone, I: storm structure. Mon. Wea. Rev., 105, 1119-1135.

Frank, W. M., 1977b: The structure and energetics of the tropical cyclone, II: dynamics and energetics. Mon. Wea. Rev., 105, 1136-1150.

Fujita, T. T., and J. J. Tecson, 1974: A kinematic analysis of tropical storm base on ATS cloud motion. SMRP Research Paper #125, The University of Chicago, 20 pp.

Gentry, R. C., E. Rodgers, J. Steranka, and W. Shenk, 1980: Predicting tropical cyclone intensity using satellite measured equivalent blackbody temperatures of cloud tops. Mon. Wea. Rev., 108, 445-455.

Gray, W., 1975: Tropical cyclone genesis. Atmos. Sc. Paper No. 234, Colorado State University, 119 pp.

Gray, W. M., 1979: Hurricanes/their formation, structure and likely role in the tropical circulation. Quart. J. Roy. Meteor. Soc., 105, 155-218. (Proceeding of Conf. of Meteor. over the Trop. Oceans).

Hasler, A. F., 1981: Stereographic observations from geosynchronous satellites: an important tool for the atmospheric sciences. Bull. Amer. Meteor. Soc., 62, 194-212.

Hasler, A. F., and E. B. Rodgers, 1977: An error analysis of tropical cyclone divergence and vorticity fields derived from satellite cloud winds on the atmospheric and oceanographic information processing system (AOIPS) Preprints, 11th Tech. Conf. on Hurricanes and Tropical Meteorology, AMS, Boston, MA, 670-675.

Hasler, A. F., W. C. Skillman, W. E. Shenk, and J. Steranka, 1979: In Situ aircraft verification of the quality of satellite cloud winds over oceanic regions. J. Appl. Meteor., 1?, 1481-1489.

Hawkins, H. F., 1976: A brief comparison of some of the conditions attending hurricanes Carmen and Fifi (1974). NOAA Tech. Memo, ERL WMPO-31, 8 pp.

Hawkins, H. F., and S. M. Imbembo, 1976: The structure of a small, intense hurricane-Inez, 1966. Mon. Wea. Rev., 104, 418-442.

Hawkins, H. F., and D. T. Rubsam, 1968: Hurricane Hilda, 1964: II. Structure and budgets of the hurricane on October 1, 1964. Mon. Wea. Rev., 99, 427-435.

Hebert, P. J., 1976: Atlantic hurricane season of 1975. Mon. Wea. Rev., 104, 453-465.

Holliday, C. R., 1977: On the rapid intensification of typhoons. Master Thesis Texas A&M University, 87 pp.

Howard, R. A., J. E. Matheson, and D. W. North, 1972: The decision to seed hurricanes. Science, 176, 1191-1202.

Jordan, E. S., 1952: An observational study of the upper wind-circulation around tropical storms. Journ. of Meteor., 9, 340-346.

Kidder, S. Q., W. M. Gray, and T. H. Vonder Haar, 1980: Tropical cyclone outer surface winds derived from satellite microwave sounder data. Mon. Wea. Rev., 108, 144-152.

Kidder, S. Q., W. M. Gray, and T. H. Vonder Haar, 1978: Estimating tropical cyclone central pressure and outer winds from satellite microwave data. Mon. Wea. Rev., 106, 1458-1464.

LaSeur, N. W., and H. F. Hawkins, 1963: An analysis of hurricane Cleo, (1958) based on data from research reconnaissance aircraft. Mon. Wea. Rev., 91, 694-709.

Lawrence, M. B., 1978: Atlantic hurricane season of 1977. Mon. Wea. Rev., 106, 534-545.

Lawrence, M. B., 1979: Atlantic hurricane season of 1978. Mon. Wea. Rev., 107, 477-491.

Lopez, R. E., 1973: Cumulus convection and larger scale circulations, I. Broadscale and mesoscale considerations, II. Cumulus and Mesoscale interactions. Mon. Wea. Rev., 101, 839-870.

McBride, J. L., 1979: Observational analysis of tropical cyclone formation. Atmos. Sc. Paper No. 308, Colorado State University, 230 pp.

McBride, J. L., and W. M. Gray, 1978: Mass divergence in tropical weather systems, Paper I: Diurnal variation; Paper II: Large scale controls on convection. Atmos. Sc. Paper No. 299, Colorado State University, 109 pp.

Numez, E., and W. M. Gray, 1977: A comparison between West Indies hurricanes and Pacific Typhoons. Preprints, 11th Tech. Conf. on Hurricanes and Tropical Meteorology, AMS, Boston, MA, 528-534.

Peslen, C. A., 1980: Short-interval SMS wind vector determinations for a severe local storm area. Mon. Wea. Rev., 108, 1407-1418.

Riehl, H., 1954: Tropical meteorology. McGraw-Hill Book Comp. Inc., New York, 392 pp.

Riehl, H. and J. Malkus, 1961: Some aspects of hurricane Daisy, 1958. Tellus, 13, 181-213.

Rodgers, E. B., and R. F. Adler, 1981: Tropical cyclone rainfall characteristics as determined from a satellite passive microwave radiometer. Mon. Wea. Rev., 109, 506-521.

Rodgers, E. B., R. C. Gentry, W. E. Shenk, and V. Oliver, 1979: The benefits of using short-interval satellite images to derive winds for tropical cyclones. Mon. Wea. Rev., 107, 575-584.

Sadler, J. C., 1976: Tropical cyclone initiation by the tropical upper tropospheric trough. Mon. Wea. Rev., 104, 1266-1278.

Smith, C. L., 1975: On the intensification of hurricane Celia (1970). Mon. Wea. Rev., 103, 131-147.

Zehr, R., 1976: Tropical disturbances intensification. Atmos. Sc. Paper No. 259, Colorado State University, 19 pp.

FIGURE CAPTIONS

Figure 1. (a) Cirrus level wind field (wind speed in knots) derived from GOES-1 for hurricane Anita at 1600 GMT, 1 September 1977, (b) the objectively smoothed analyzed wind field (0.4 km spacing) using the Lackman technique, (c) the radial, and (d) tangential wind component of the derived winds. See text for further explanation.

Figure 2. (a) Mean radial wind profile derived from the composite rawinsonde data at 444 km radius from the center for the western Atlantic hurricanes adapted from McBride (1979) (b) a simplified model of McBride's (1979) radial wind profile.

Figure 3. Time history of tropical cyclone Caroline's maximum winds (dashed) and central pressure (solid) during the period of 28 August to 1 September, 1975. Arrows indicate time of satellite observations.

Figure 4. Streamline analyses of tropical cyclone Caroline's (a) lower and (b) upper tropospheric environmental wind field derived from 0000 GMT 30 August 1975 observed 850 and 200 mb rawinsonde data, respectively, together with the satellite-derived winds (not shown) that were extrapolated to the rawinsonde time. Wind speed in knots.

Figure 5. SMS-2 derived winds of tropical cyclone Caroline at the (a) cumulus cloud base and (b) cirrus level at 1600 GMT 29 August, 1975. Otherwise the same notation as in Fig. 1a.

Figure 6. Time history of tropical cyclone Anita's maximum winds and central pressure for the period 30 August to 3 September, 1977. Otherwise the notation is the same as in Fig. 3.

Figure 7. Streamline analyses of tropical cyclone Anita's (a) lower and (b) upper tropospheric environmental wind field at 1200 GMT 31 August, 1977. Otherwise the notation is the same as in Fig. 4.

Figure 8. GOES-1 derived winds of tropical cyclone Anita's (a) lower and (b) upper tropospheric environment at 1600 GMT 31 August, 1977. Otherwise the notation is the same as in Fig. 1a.

Figure 9. GOES-1 derived winds at the cumulus cloud base level for tropical cyclone Anita 1300 GMT 30 August, 1977. Dot represents the center of lower tropospheric circulation. Otherwise notation same as in Fig. 1a.

Figure 10. GOES-1 derived winds at the cirrus level for tropical cyclone Anita 1300 GMT 30 August. 1977. Otherwise notation is the same as in Fig. 1a.

Figure 11. Horizontal divergence field calculated from GOES-1 derived winds at the cirrus level for tropical cyclone Anita 1300 GMT 30 August, 1977. Dashed (solid) lines represent horizontal convergence (divergence). Otherwise notation is the same as in Fig. 1a.

Figure 12. GOES-1 derived winds at the cirrus level for tropical cyclone Anita 1600 GMT 30 August, 1977. Otherwise notation is the same as in Fig. 1a.

Figure 13. GOES-1 derived winds at the cirrus level for tropical cyclone Anita 1900 GMT 30 August, 1977. Otherwise notation is the same as in Fig. 1a.

Figure 14. Time history of tropical cyclone Ella's maximum winds and central pressure during the period of 1-4 September, 1978. Otherwise notation is the same as in Fig. 3.

Figure 15. Streamline analysis of tropical cyclone Ella's (a) lower and (b) upper tropospheric environmental wind field at 1200 GMT 2 September, 1978. Otherwise notation is the same as in Fig. 4.

Figure 16. GOES-1 wind of tropical cyclone Ella at the (a) cumulus cloud base and (b) cirrus level at 1600 GMT 2 September, 1978. Otherwise notation is the same as in Fig. 1a.